

Adsorptive Removal of Anthracene from Water by Biochar Derived Amphiphilic Carbon Dots Decorated with Chitosan

Farzad Hashemzadeh^{1,a}, Maede Esmaeili Khoshmardan², Daryoush Sanaei^{2*,a}, Mohammad Rezvani Ghalhari³, Hamidreza Sharifan⁴, Vassilis J. Inglezakis⁵, Javier A. Arcibar-Orozco⁶, Wasim Akram Shaikh⁷, Eakalak Khan⁸, Jayanta Kumar Biswas^{9*}

¹Water and Wastewater Research Center, Water Research Institute, Tehran, Iran

²Department of Environmental Health Engineering, Faculty of Public Health and Safety, Shahid Beheshti University of Medical Science, Tehran, Iran

³Department of Environmental Health Engineering, Faculty of Public Health and Safety, Shahid Beheshti University of Medical Science, Tehran, Iran

⁴Department of Natural Science, Albany State University, Georgia, USA

⁵Department of Chemical & Process Engineering, University of Strathclyde, UK

⁶Research Department, CIATEC A.C. Centro de Innovación Aplicada en Tecnologías Competitivas, León, Mexico

⁷Department of Basic Sciences, School of Science and Technology, The Neotia University, Sarisha, South 24 Parganas, West Bengal, India – 743368

⁸Civil and Environmental Engineering and Construction Department, University of Nevada, Las Vegas, Las Vegas, NV 89154-4015, USA

⁹Enviromicrobiology, Ecotoxicology and Ecotechnology Research Laboratory (3E-MicroToxTech Lab), International Centre for Ecological Engineering, Department of Ecological Studies, University of Kalyani, Kalyani, Nadia, West Bengal - 741235, India

* Corresponding Author (Jayanta Kumar Biswas, email: jkbiswas@klyuniv.ac.in)

^a: "These authors contributed equally"

This is a peer-reviewed, version of record of the following paper: Hashemzadeh, F., Khoshmardan, M. E., Sanaei, D., Ghalhari, M. R., Sharifan, H., Inglezakis, V. J., Arcibar-Orozco, J. A., Shaikh, W. A., Khan, E., & Biswas, J. K. (2024). Adsorptive removal of anthracene from water by biochar derived amphiphilic carbon dots decorated with chitosan. *Chemosphere*, 352, Article 141248. Advance online publication. <https://doi.org/10.1016/j.chemosphere.2024.141248>

32 Abstract

33 Anthracene belongs to the polycyclic aromatic hydrocarbon (PAH) consisting of benzene rings,
34 unusually highly stable through more π -electrons and localized π -bond in entire rings. Aqueous-
35 phase anthracene adsorption using carbon-based materials such as biochar is ineffective. In this
36 paper, carbon dots (CDs) derived from the acid treatment of coconut shell biochar (CDs/MCSB)
37 decorated with chitosan (CS) are successfully synthesized and applied for anthracene removal
38 from aqueous solutions. The *h*-CDs/MCSB exhibited fast adsorption of anthracene with significant
39 sorption capacity ($Q_{max} = 49.26 \text{ mg g}^{-1}$) with 95% removal efficiency at 60 min. The study
40 suggested chemisorption dominated monolayer anthracene adsorption onto *h*-CDs/MCSB, where
41 a significant role was played by ion-exchange. Density Functional Theory (DFT) suggested the
42 anthracene adsorption was dominated by the electrostatic interactions and delocalized electron,
43 induced by higher polarizability of functional groups on the surface of hybrid CDs/MCSB assisted
44 by chitosan (*h*-CDs/MCSB). In addition, the aromatic structure of CDs/MCSB and high
45 polarizability of functional groups provided the strong interactions between benzene rings of
46 anthracene and hybrid adsorbent-assisted multiple π -bond through delocalized π -bond and
47 polarization-induced H-bond interactions. The presence of carboxylic and sulfonic groups on the
48 CDs/MCSB surface also contributed to the effective adsorption of anthracene was confirmed by
49 the fluorescence spectra. The results showed that the hybrid adsorbent was an effective material
50 for removing PAHs, usually difficult to remove from water owing to the presence of benzene rings
51 in their structures. Further, consistency in the DFT results suggested the outstanding binding
52 capacity with the anthracene molecules with *h*-CDs/MCSB.

53

54 **Keywords:** Polycyclic aromatic hydrocarbon; Anthracene, Adsorption; Chitosan-biochar;
55 Polarizability of functional groups

56

57

58

59

60

61

62 **1. Introduction**

63 A class of emerging contaminants that recently have been more noticed is polycyclic aromatic
64 hydrocarbons (PAHs). This class of pollutant has recently gained more interest among researchers
65 owing to its potential threat to the ecosystem and human health. Recently, PAHs emissions have
66 become a major problem in some developed and developing countries(Gupta 2018; Zango et al.
67 2019). There is a multifarious pathway for introducing PAHs into environmental media,
68 particularly in waterbodies, including discharges from municipal wastewater treatment plants and
69 petrochemical industries, the release of petroleum products, and leakage of engine oils (Zhang,
70 Chen, et al. 2018; Imam et al. 2021). Among the PAHs, anthracene is considered to be one of the
71 ~~the~~ most toxic, which has recently been detected widely in multitudinous environmental samples,
72 particularly in foods, water, waterbodies, and sewage sludge (Ma et al. 2021).

73 (Amorini et al. 2022) reported anthracene is highly resistant not only to biodegradation but
74 also the conventional physicochemical techniques among the PAHs resulting into some serious
75 health issues, including cardiovascular disorders, lung cancer, and defects in reproductive systems,
76 can be related to PAHs like anthracene. The PAHs compounds have been classified into three
77 major groups as (a) endocrine disruptors, (b) carcinogenic, and (c) mutagenic by the United States
78 Environmental Protection Agency (USEPA) (Zhang et al. 2022). Their removal from waterbodies
79 demands the development of effective methods(Ma et al. 2021; Wiśniowska and Włodarczyk-
80 Makuła 2022; Pathak et al. 2022). Several treatment methods have been adopted for the effective
81 purifying anthracene from polluted-based media, such as biological treatment, coagulation,
82 flocculation, and catalytic degradation(Zhou et al. 2022). However, most of these methods suffer
83 from incomplete elimination, owing to toxicity and the presence of a long chain of carbon,
84 resulting in the persistence to the microorganisms for biodegradation. Cost and toxic effects of the
85 chemical methods are among the major problems associated with the chemical treatment of
86 PAHs(Shaikh, Islam, and Chakraborty 2021; Ajani et al. 2022).

87 Among the treatment techniques, the adsorption process is a promising method to purify
88 the PAHs-laden aqueous media due to its easy operation, high efficiency, and cost-effectiveness.
89 Moreover, the adsorption process could be used as a pretreatment method to remove PAHs like
90 anthracene. Anthracene harms aquatic life, poisons fish, invertebrates, and algae, affecting their
91 development, reproduction, and health; also, can accumulate in aquatic creatures may multiply

92 along the food chain, causing ecological instability. Waterborne anthracene can damage
93 ecosystems and reduce biodiversity (Le Bihanic et al. 2015). Ingestion or water contamination
94 with anthracene may be harmful. Long-term anthracene exposure can cause rashes, respiratory
95 issues, and cancer. Health and safety are threatened by anthracene in water (Ojha and Tiwary
96 2021). Regulatory bodies and environmental groups have devised water anthracene pollution
97 standards to reduce its risk. Remediating anthracene-contaminated water using physical,
98 chemical, or biological approaches reduces its environmental and health impacts (Singh and Singh
99 2023). Among the multifarious adsorbent materials, carbon-based materials are well suited owing
100 to high chemical stability, various biomass and non-biomass precursors, thermal stability, ease of
101 operation and recovery, low cost, and availability (Ahmed, Hameed, and Hummadi 2020;
102 Dehghani et al. 2016; Chen, Gao, et al. 2022; Lopes and Astruc 2021). Multifarious and
103 multitudinous biomass and waste materials-based materials like carbon nanotube (CNT) and
104 graphene are the most significant and widely utilized adsorbents for the anthracene as well.

105 In this study, we have derived a functional matrix, biochar, from one of the most significant waste
106 biomasses, coconut shells. It is a potential agricultural waste worldwide (Dai et al. 2021; Shaheen
107 et al. 2022; Li, Shaheen, et al. 2022). Because of its unique characteristics, coconut shell-based
108 biochar is used for various applications, including the treatment of a wide range of environmental
109 pollutants like PAHs. For example, Atibun Isa et al, synthesized a functionalized-coconut shell
110 biochar to remove Hg (II) from solution. Their results exhibited that functionalization biochar can
111 remove Hg (II) effectively and faster compared to the pristine biochar (Isa et al. 2022). In addition,
112 the removal of antibiotics from wastewater using recyclable coconut shell-based biochar was
113 improved by activated with KOH and magnetified with FeCl₃ (Sun et al. 2022). The study
114 indicated the outpacing of effectively adsorbed antibiotics on modified biochar was due to the
115 hydrogen bonding. However, the anthracene consists of three fused benzene rings together, their
116 adsorption by the biochar only is not effective specifically due to the lipophilicity of anthracene
117 and the presence of π -electron clouds (Kundu and Gupta 2007).

118 The biochar surface is enhanced with oxygen-containing functional groups through acid treatment.
119 These functional groups act as active sites for the sorption of PAHs, utilizing mechanisms such as
120 π - π interactions and hydrogen bonding (Valizadeh et al. 2022). The process of acid-induced
121 etching and oxidation leads to the formation of meso- and micropores in the biochar structure,

122 which increases its surface area and creates more sites for the adsorption of PAHs (Gholami et al.
123 2021). By deliberately introducing acidic functional groups, the process becomes capable of
124 selectively targeting particular PAH molecules, enabling customized elimination based on factors
125 such as molecular size, polarity, and aromaticity (Ding and Fang 2010). Acid-treated biochar
126 demonstrates increased effectiveness and specificity in eliminating PAHs from polluted settings,
127 providing a promising approach for focused remediation initiatives (Dai et al. 2019). The
128 customized structure of acid-treated biochar adheres to the tenets of green chemistry, offering an
129 environmentally acceptable and enduring method for addressing PAH contamination. The acid
130 treatment's adaptability enables the tailoring of biochar characteristics to match various matrices
131 polluted with PAHs, while also facilitating scalability for practical use (Adeola and Forbes 2021).

132 Biochar modification can be a promising strategy to eliminate anthracene due to its porosity
133 and the presence of numerous active surface functional groups, including OH, CH, CH_x, C=C,
134 C=O, C-O-C, NH_x, and SH. In addition, the presence of stable benzene ring and the lower
135 adsorption capacity of anthracene made to unveil a modified biochar with precise insight into
136 interaction mechanisms. Hence, in this study, a coconut shell-derived sulfonated biochar is
137 successfully synthesized. The acid treatment of coconut shell biochar (MCSB) leads to the
138 formation of carbon dots (CDs) consisting of functionalized sulfonic acid, carboxylic acid, as well
139 as hydroxyl epoxy and carbonyl groups on their surface (Usman et al. 2021; Huang et al. 2016).
140 The acid treatment of biochar entails the application of potent acids to corrode the surface of the
141 biochar, resulting in the formation of pores and an augmentation of the surface area (Wang and
142 Wang 2019). Furthermore, the use of acid treatment causes chemical alterations in biochar,
143 resulting in the incorporation of functional groups like carboxylic and phenolic moieties onto the
144 surface of the biochar (Zhang, Xu, et al. 2018).

145 Beyond those advantages of CDs/MCSB adsorbent, the acid modification of coconut shell biochar
146 may lessen or even degenerate some weak functional groups on the adsorbent as well as weaken
147 the binding of active groups with anthracene (Wu et al. 2022; Saheed, Da Oh, and Suah 2021;
148 Usman et al. 2021). The benzene rings of anthracene have an insignificant affinity to interact with
149 functional groups of adsorbents, including CDs/MCSB. To address this inadequacy, an
150 environmental-friendly natural polysaccharide-based material, chitosan (CS) was developed and
151 used as the functional material for CDs to produce eco-friendly, target-specific, highly efficient,

152 and low-cost CDs decorated hybrid polysaccharide-based chitosan nanocomposite (*h*-
153 CDs/MCSB).

154 This study assessed the potency of the *h*-CDs/MCSB for enhanced removal of anthracene, keeping
155 the 'waste to wealth' principle in mind. The biogenic *h*-CDs/MCSB was tailor-made to target
156 anthracene and potentially similar contaminants. The synthesis of amphiphilic carbon dots
157 generated from biochar is cost-effective, as it entails converting biomass waste materials into
158 valuable goods (Zhu et al. 2021). The ample availability of biomass sources additionally enhances
159 the economic feasibility of this approach. Furthermore, the utilization of chitosan, derived from
160 sources like crab shells, offers a cost-efficient substitute for synthetic polymers (Junceda-Mena,
161 García-Junceda, and Revuelta 2023; Hashmi et al. 2022). When evaluating the long-term
162 advantages of water remediation, the cost-effectiveness of this technique becomes apparent,
163 particularly when compared to conventional remediation approaches that may entail greater
164 operational and maintenance costs. The objectives of the study are: (a) fabricate biogenic carbon
165 dots from the acid-treated waste coconut shell-derived biochar, (b) elucidate the in-depth charge
166 balancing with stabilization mechanism, and (c) implement the developed adsorbent with
167 multifarious active groups for anthracene removal form aqueous solutions.

168

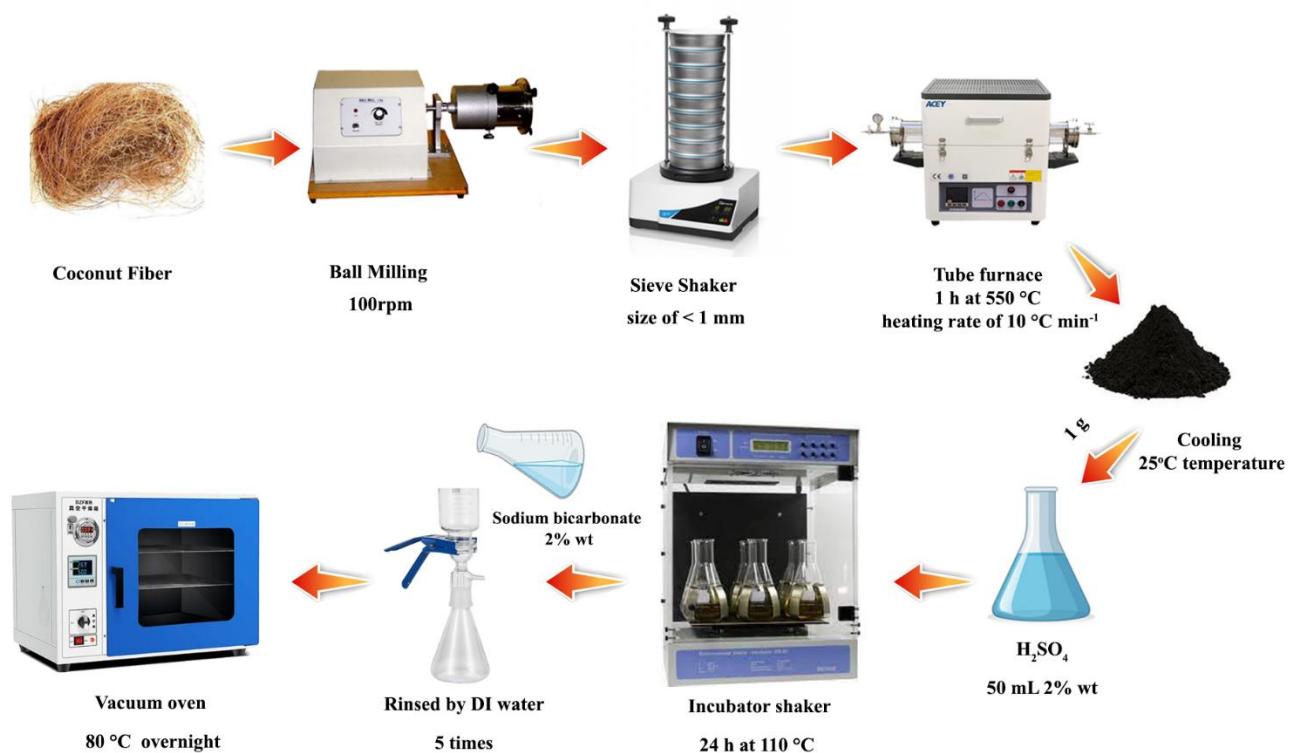
169 **2. Material and Methods**

170 **2.1.Preparation of carbon dots decorated biogenic chitosan nanocomposite**

171 Biochar is prepared by simple carbonization and then activation of the coconut shell. The overall
172 process of synthesis is shown in Scheme 1. Firstly, coconut shell was procured from a tropical fruit
173 market (Fruit and vegetable store, Tehran, Iran), washed thoroughly with tap water followed by
174 distilled water, and oven dried at 105 °C for 48 h for dehydration. A ball milling with a rotating
175 speed of 100 rpm was carried out for grinding coconut shells. The resulting powder was sized
176 using a sieve shaker to obtain an average particle size of < 1 mm. The carbonization was performed
177 by pyrolyzing dried coconut shells in a tube furnace for 1 h at 550 °C with a heating rate of 10 °C
178 min⁻¹(Qu et al. 2021; Gurav et al. 2021). After cooling to ambient temperature, the resulting
179 product (1 g) was added with 50 ml 2% wt. H₂SO₄ solution and allowed to react for 24 h at 110
180 °C in a temperature-controlled incubator shaker (Incubator ES 20/60, bioSan) to activate the

181 carbonized coconut shell. The required mixture was washed with 2% sodium bicarbonate solution
 182 to remove unbound acid and then several times with distilled water. Finally, the resulting carbon
 183 dots (CDs) modified coconut shell biochar (CDs/MCSB) were dried at 80 °C in a vacuum oven
 184 overnight.

185 The *h*-CDs/MCSB was synthesized by adding chitosan to 0.5 % wt. acetic acid under strong
 186 stirring (100 rpm) for 24 h. After that, chitosan was added with a ratio of 5 to 1 (w/w) than of
 187 CDs/MCSB and continued stirring for another 24 h to achieve CDs-MCSB adorned CS (*h*-
 188 CDs/MCSB). This process was repeated three times, and finally, the *h*-CDs/MCSB was washed
 189 with distilled water and dried at 80°C in a vacuum oven.



190

191

192

193

194

195

196 2.2.Characterization

197 The functional groups of the *h*-CDs/MCSB were examined by Fourier transform infrared
 198 spectroscopy (FTIR) (Nicolet, 6700, Thermo fisher, USA). The surface morphology of the *h*-
 199 CDs/MCSB was studied using Field emission scanning electron microscopy (FE-SEM). Raman
 200 spectra were carried out at 532 nm using a micro spectrometer (LabRAM HR800, Horiba Jobin-
 201 Yvon, Japan). The Brunauer-Emmett-Teller (BET) adsorption-desorption isotherm analysis was
 202 used to investigate the porosity ($\text{cm}^3 \text{g}^{-1}$), pore diameter (nm), and specific surface area ($\text{m}^2 \text{g}^{-1}$) of
 203 the *h*-CDs/MCSB (TrisStar II 3020 analyzer). The X-ray Diffraction (XRD) analysis was
 204 performed using STOE-STADV to determine the structure and mineralogical composition of the
 205 *h*-CDs/MCSB using Cu-K α monochromatic radiation at 1.54 Å. A thermogravimetric analysis
 206 (Shimadzu TGA-50 Analyzer) was performed at a heating rate of 10 °C min⁻¹ to understand the
 207 thermal stability of the *h*-CDs/MCSB. The CDs were detected using a Horiba fluorolog
 208 fluorescence spectrometer after separating them by sonicating 50 mg of acid treatment coconut
 209 shell biochar in 20 ml of 2-propanol for 3 h and removing MCSB by filtration (Fig. S1).
 210 pH of aqueous solution was measured with a pH meter (Metrohm, lab pH meter, Model 827).

211

212 2.3.Isotherm and kinetics models

213 The Langmuir and Freundlich isotherm models were investigated, to determine the anthracene
 214 uptake mechanism using *h*-CDs/MCSB. (Baharum et al. 2020; Dehghani et al. 2019; Madikizela
 215 2021; Khader et al. 2022)

$$216 \frac{C_e}{q_e} = \frac{1}{K_L Q_{max}} + \frac{C_e}{Q_{max}} \quad (1)$$

217

$$218 \ln q_e = \ln k_F + \frac{1}{n_F} \ln C_e \quad (2)$$

219 Where, C_e is equilibrium anthracene concentration (mg L^{-1}), q_e is adsorbed amount at equilibrium
 220 in mg/g^{-1} , Q_{max} is maximum adsorption capacity (mg g^{-1}), K_L is Langmuir constant (L mg^{-1}), n_F is
 221 Freundlich adsorption strength, and K_F is Freundlich adsorption capacity.

222 Moreover, to investigate the favorability of *h*-CDs/MCSB based on Langmuir isotherm, a
 223 dimensionless constant (R_L) was calculated according to the following equation (Javanbakht and
 224 Rafiee 2022) :

$$R_L = \frac{1}{1+C_0K_L} \quad (3)$$

Where, K_L and C_0 are the Langmuir constant and the initial anthracene concentration, respectively.

The range of R_L between 0 and 1 represents the favorability of the process.

The adsorption kinetics of *h*-CDs/MCSB were further investigated using pseudo-first order and pseudo-second order models, as respectively given as (Chen, Hoang, et al. 2022; Zhang et al. 2021; Xue et al. 2021):

$$\ln(q_e - q_t) = \ln(q_e) - k_1t \quad (4)$$

$$\frac{t}{q_t} = \frac{1}{K_2q_e^2} + \frac{t}{q_e} \quad (5)$$

Here, q_e , q_t , K_1 , and K_2 are equilibrium anthracene concentration (mg g^{-1}), anthracene concentration at time t (mg g^{-1}), rate constant of pseudo-first and rate constant of pseudo-second order models, respectively.

239

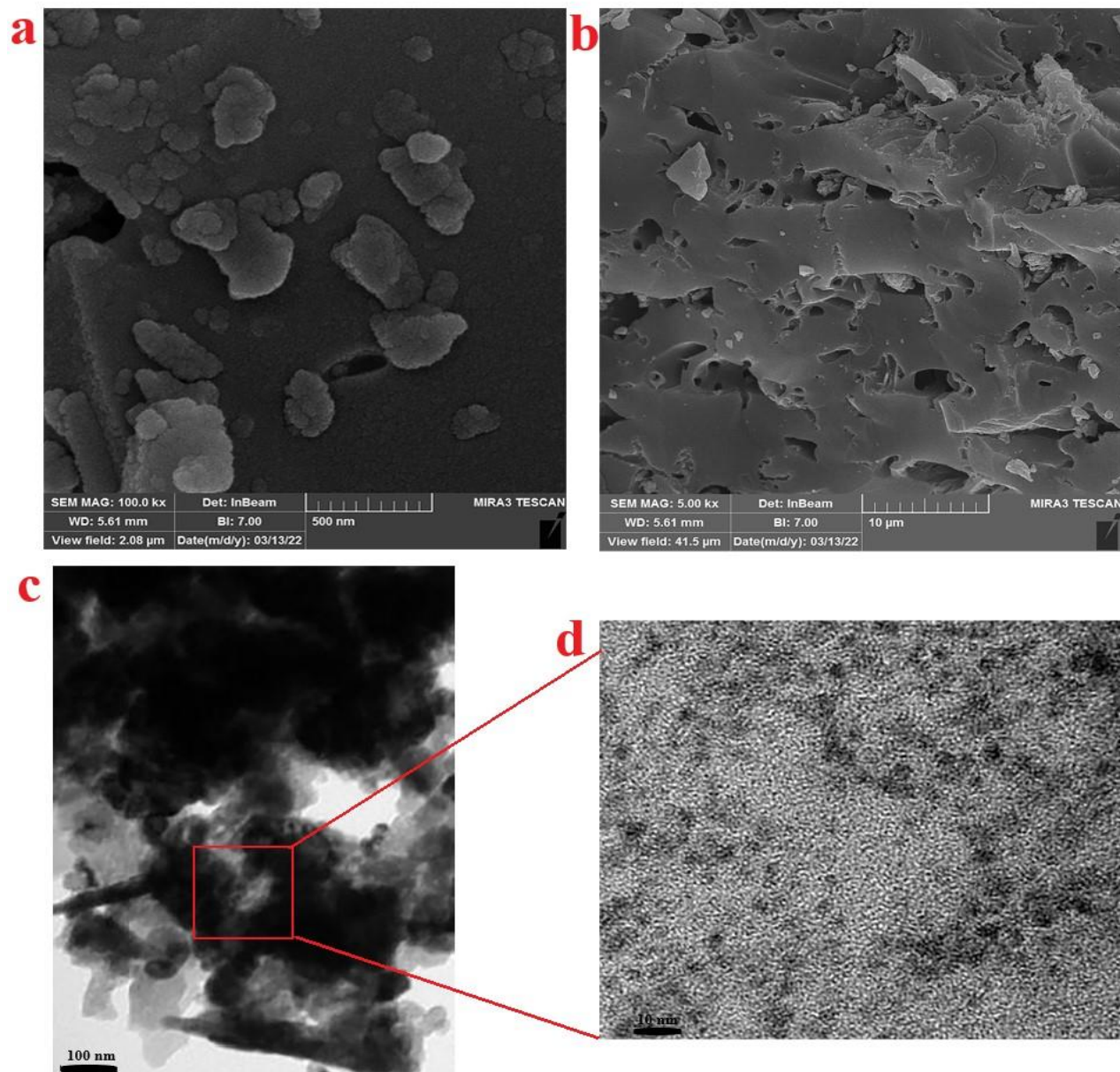
240 3. Results and Discussion

241 3.1. Structural characterization

242 The morphology of *h*-CDs/MCSB before and after sulfonation and hybridizing with chitosan
 243 exhibited a heterogeneous porous structure (Fig. 1a and 1b). Acid treatment changed the porous
 244 structure towards multifarious pores. In this study, the acid treatment resulted in the generation of
 245 micro and mesopores structured matrix. The co-presence of micro and mesoporous structures in
 246 *h*-CDs/MCSB provides higher adsorption sites through easy diffusion of anthracene to the surface
 247 of the adsorbent(da Silva Medeiros et al. 2022). Fig. 1c and 1d, show that the sulfonation of
 248 coconut shell biochar created a dispersed layer of CDs in the range of 3-5 nm over the adsorbent.
 249 CDs dispersed on the coconut shell biochar can act as a functional supporting material with
 250 favorable structure, including enriched active surface functional groups and high surface area. In
 251 addition, CS could stabilize active groups of CDs adorned MCSB, strengthen the structure, and
 252 chelate sites for adsorption reactions(Mobarak, Ali, and Seliem 2021; Verma et al. 2022;
 253 González-González et al. 2022; Liu et al. 2021; Mansuriya and Altintas 2021; Inbaraj, Sridhar,

254 and Chen 2021). It is important to note that both dispersed CDs and CS adorned coconut shell
 255 biochar would act as the active components of the adsorbent material.

256 **Fig. 1: FE-SEM of (a) CDs/MCSB and (b) CS adorned hybrid CDs/MCSB; and (c) and (d)**



257 **TEM images of CS adorned hybrid CDs/MCSB**

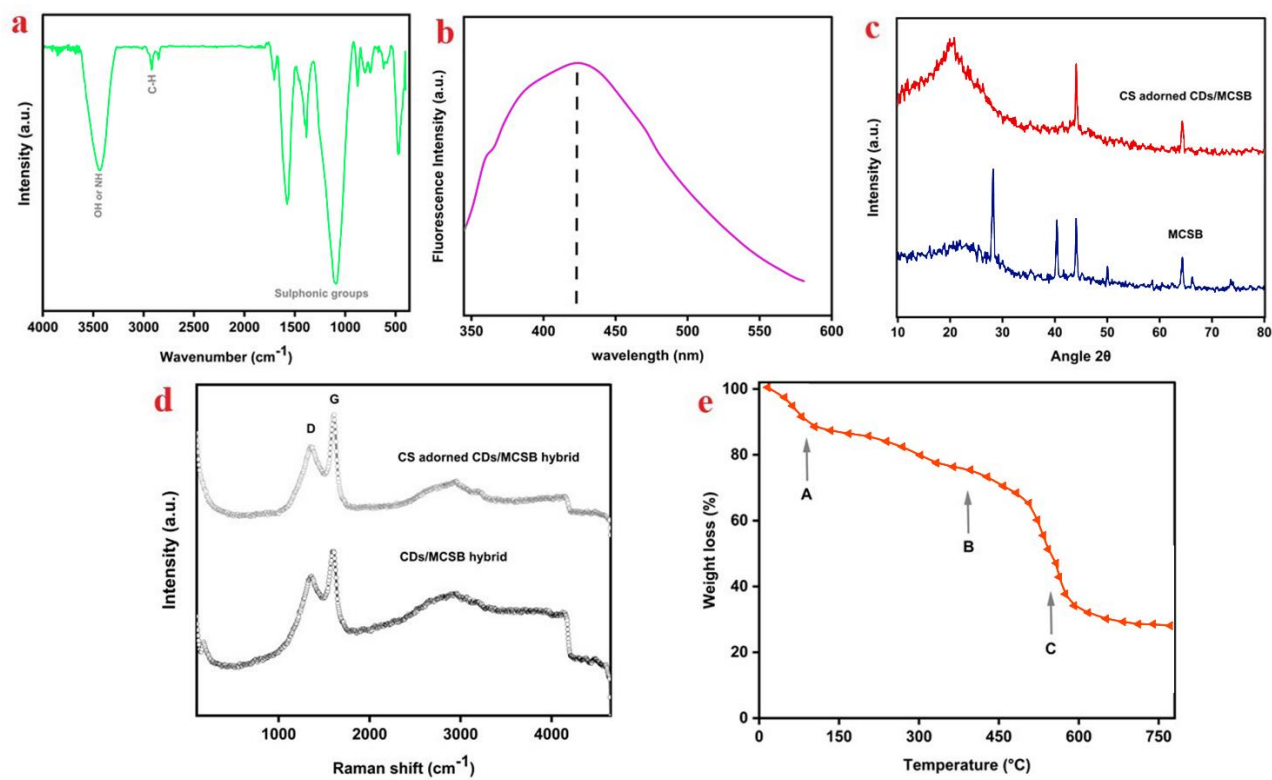
258 The co-presence of sulfonic groups in CDs and coconut shell biochar, as well as other
 259 active groups, was verified via FTIR spectra (Fig. 2a), with details being presented in Table S1.
 260 Further, CDs formation was quantified using fluorescence emission spectra. As shown in Fig. 2b,
 261 the strong intensity at 434 nm pertaining to CDs response agreed with the literature (Li et al. 2021;

262 Feng et al. 2021). As well shown in Fig. 2c, several strong and sharp peaks were at 27.8 °, 41.2°,
263 and 44.6° for MCSB, representing to atomic arrangements and graphene-like structures (Mirzaee
264 and Sartaj 2022). By adorning it with CS and the presence of CDs, the broad and weak crystalline
265 peaks appeared that the presence of multifarious active groups that could be created various
266 bonding such as H-bonding with anthracene molecules and also the generating the regularity in
267 hybrid adsorbent (Okoro et al. 2022). The structural characteristics of *h*-CDs/MCSB, including
268 chemical bond vibration and cation distortion, were characterized using Raman spectroscopy. The
269 Raman spectra showed prominent peaks at 1354 cm⁻¹ (D peak) ascribed to the A_{1g} symmetry
270 vibration of sp² hybridized carbon atoms or defect (or disorder) in carbon structure and at 1585
271 cm⁻¹ (G band) tied to the E_{2g} symmetry vibration of sp² carbon atoms in the graphite structure (Fig.
272 2d) (Palansooriya et al. 2021; Wang et al. 2021). The calculated I_G/I_D ratio of the *h*-CDs/MCSB
273 was 1.32, which is 15% higher than that of the coconut shell biochar (1.15), indicating enhanced
274 graphitization degree in the *h*-CDs/MCSB. All of the spectra were apparently consistent,
275 confirming high graphitization and good electrical conductivity of the *h*-CDs/MCSB. This
276 suggests that the introduction of CS could facilitate charge transfer between adsorbate and
277 adsorbent and also delocalized electrons over *h*-CDs/MCSB that stabilize functional groups and
278 subsequently enhance the multifarious mechanisms in the adsorption of anthracene.

279 To elucidate the underlying mechanism of the anthracene adsorption on the textural
280 properties of the novel composite, N₂ adsorption-desorption tests were conducted (Fig. S2).
281 According to the IUPAC classification, the type-IV isotherm was observed for *h*-CDs/MCSB,
282 suggesting the existence of micro/mesopores structures. The CS exhibited a very low BET specific
283 area of 24.34 m² g⁻¹, whereas the CDs-derived coconut shell biochar exhibited a 412.01 m² g⁻¹ with
284 a pore volume of 0.184 cm³ g⁻¹ (Table S3). The reduction in the surface area of the *h*-CDs/MCSB
285 could be ascribed to the modification with CS by introducing the functional groups, in particular,
286 -NH₂ groups, which would occupy some of the vacant pore space (especially microporous
287 moieties) in the CDs/MCSB. The pore distribution of *h*-CDs/MCSB ranged between 1.15 and 3.5
288 nm, while the *h*-CDs/MCSB extended this range towards mesopores ranges (1.47 to 5.9 nm).

289 The stability of as-prepared material under different temperatures was investigated by the
290 TGA analysis, as shown in Fig. 2e. The first stage (A) of weight loss, with about 16%, is attributed
291 to the release of light volatile chemicals and physically adsorbed interlayer-bound water. The

292 further weight loss corresponded to the partial decomposition of (hemi)cellulose and the
 293 disappearance of structural water molecules (Shaikh et al. 2020) of the *h*-CDs/MCSB (B). In the
 294 third step (C), a moderate weight loss was observed, likely due to the decomposition of residual
 295 carbonaceous materials and large phytochemicals like lignin (Shaikh, Islam, and Chakraborty
 296 2021). The decomposition of *h*-CDs/MCSB resulted from the splitting of the butyric acid, forming
 297 acetic, glycosidic bonds, and probably lower fatty acids (Chen, Gao, et al. 2022).



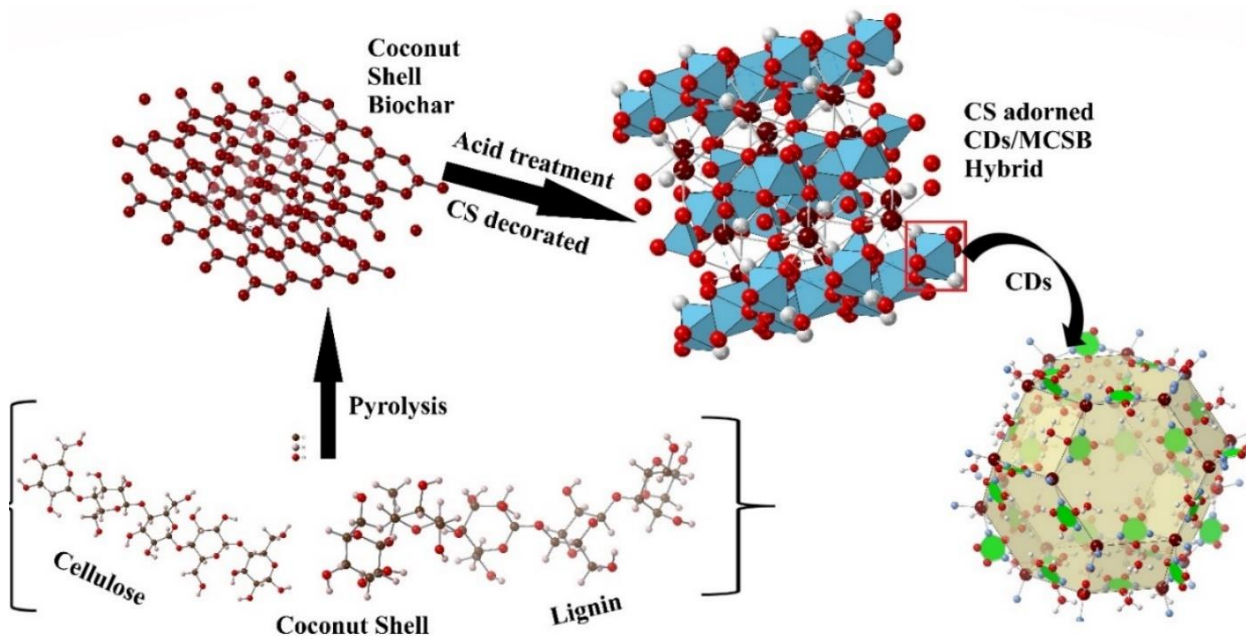
298
 299 **Fig. 2: (a) FTIR spectra of as-prepared adsorbent hybrid; (b) Fluorescence emission spectra**
 300 **of formed CDs; (c) the XRD pattern of as-prepared adsorbent; (d) Raman spectra of as-**
 301 **synthesized hybrid adsorbent; and (e) the thermal stability of *h*-CDs/MCSB.**

302
 303 **3.2.The formation principle of the prepared adsorbent hybrid**

304 The coconut shell biochar was functionalized with oxygen-containing groups, in particular,
 305 sulfonic and carboxylic acid groups and carbon dots (CDs). The chitosan (CS) decorated on the
 306 hybrid CDs/MCSB formed the adsorbent hybrid with induced highly polarized functional groups
 307 that protect and stabilize the CDs at high temperatures. The scheme, representing plausible CS-

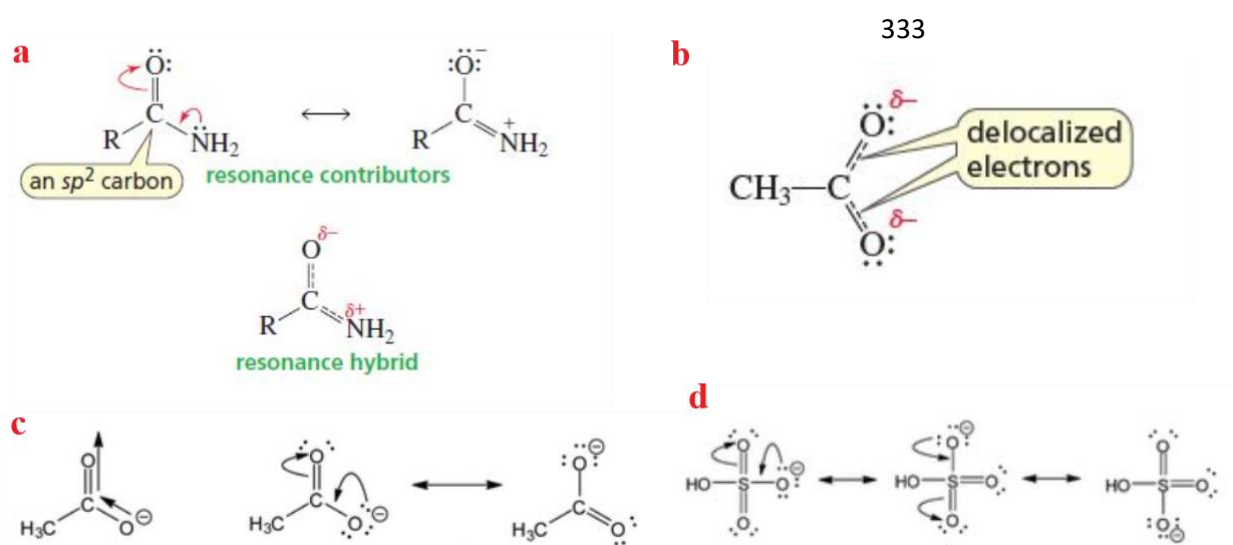
308 adorned hybrid CDs/MCSB formation, is depicted in Fig. 3. The characterization results in
 309 subsection 3.2 supports this proposed scheme.

310 Generally, coconut shells consist of a wide range of polymeric phytochemicals, including
 311 cellulose, hemicellulose, and lignin (Sun et al. 2022). After pyrolysis and removal of water, a
 312 highly and randomly aromatic compound with aggregate layers of graphene and graphite was
 313 formed (Li, Shi, and Luo 2022). The aromatic groups containing coconut shell biochar could lead
 314 to delocalizing π electrons in whole structures, considered as Lewis bases (Yuan et al. 2022; Tang
 315 et al. 2022). After undergoing oxidative acid treatment, heterogeneous, nanosized graphene-like
 316 aggregates and atomic arrangements beside the formation of the carbon dots were developed (Li,
 317 Shi, and Luo 2022). The simultaneous anchoring of oxygen-containing groups, in particular, -
 318 SO_3H and $-\text{COOH}$ groups on CDs/MCSB surface and leaching some of the acids into sensitive
 319 components of carbonaceous channels, resulting in the generation of mesoporous beside
 320 microporous structures. The incorporation of chitosan into the lattice structure of CDs/MCSB can
 321 increase delocalization energy, the polarizability of functional groups of surfaces, rich-reactive
 322 groups, and breaking the inactive groups of the sp^2 -hybridized carbon atom network.



323 **Fig. 3 The formation principle of the prepared adsorbent hybrid**

324 The increasing delocalization energy of CDs/MCSB decorated with chitosan could
 325 stabilize the active groups and form strong electrostatic and non-covalent interactions (Jiang et al.
 326 2021; Oh and Seo 2019; Chen et al. 2014). The introduction of chitosan to CDs/MCSB can increase
 327 the polarizability and delocalization energy of the adsorbent (Fig. 4). As can be seen in Fig. 2a,
 328 with the introduction of CS into a hybrid adsorbent, the -NH_2 groups of CS that have lone pair
 329 directly can attach to a benzene ring of anthracene, then the lone pair could be delocalized. This
 330 occurrence is called electron donation by resonance. As a result, electron donation could
 331 destabilize anthracene, allowing an easy interaction and bonding with the functional groups of the
 332 adsorbent.



334

335 **Fig. 4 (a) The resonance contributor and hybrid of CS adorned *h*-CDs/MCSB obtained**
 336 **moving lone-pair electrons toward an sp^2 carbon; (b) the π bonds of the COO^- groups on the**
 337 **hybrid adsorbent that are shared by two oxygens and the carbon (the dashed lines indicate**
 338 **the delocalization of two π electrons over three atoms; (c) inductive and/or in-field and**
 339 **resonance stabilization of a carboxylate base on the hybrid adsorbent; and (d) inductive**
 340 **and/or in-field and resonance stabilization of sulfonic groups functionalized on the CDs.**

341 The carbonyl groups are considered an electron-withdrawing group that withdraws
 342 electrons from the benzene ring of anthracene double bond through sigma bonds. This leaves a
 343 partial positive charge on the sp^2 carbon of anthracene rings that can probably add π electrons of
 344 carbonyl groups to the partial positive charge of carbon (Fig. 4b). The inductively electron-

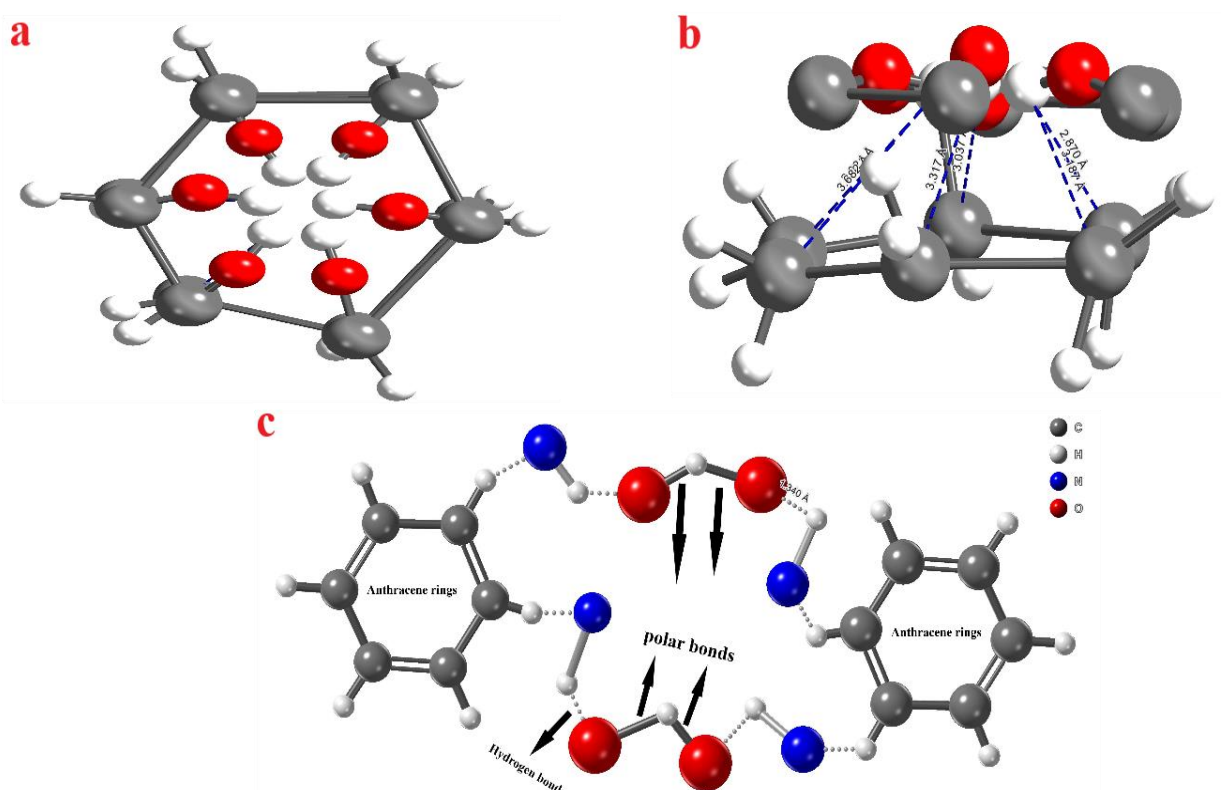
345 withdrawing C=O groups attached directly to the active center and methyl groups in carboxylate
346 groups might develop anionic oxygen atom (negative charge O), and further might stabilize the
347 anionic oxygen atoms of the carboxylate groups (Fig. 4c). This can create a conjugation between
348 π symmetry orbitals of the O=C-O- system and π symmetry orbitals of anthracene rings (π - π
349 conjugation interactions). Further, the acid treatment of coconut shell biochar and accordingly
350 generated functionalized carbon dots (CDs), which provide the HOSO₂ groups attached to the OH
351 center (Fig. 4d), are expected to be completely inductive withdrawing electrons. This can be
352 originated from the presence of high electronegative oxygen and the moderately electronegative
353 sulfur atom concomitantly.

354 According to DFT calculation, the interaction energy between anthracene and functional
355 groups of carbon dots derived from coconut shell biochar was -78.85 eV. When *h*-CDs/MCSB is
356 in an aqueous solution containing a given anthracene concentration, each functional group on the
357 adsorbent (Table S1) allows a H-atom to bind with the aromatic ring of anthracene molecules
358 (H..... π interaction) (Fig. 5a and 5b)(Gong, Li, and Li 2021; Ren et al. 2018). As can be seen
359 from characteristics analysis and DFT calculation (Fig. 5; Supplementary document), the
360 introduced CS could polarize functional groups effectively on the surface of the adsorbent, and
361 thereby the efficiency of anthracene adsorption enhanced, contributing multifarious simultaneous
362 mechanisms and active binding. Moreover, CS could create a strong and stable bonding between
363 the adsorbent's surfaces and benzene rings of anthracene through strong polarizability and electron
364 delocalization. As well known, the adsorption process depends on the adsorbent properties, such
365 as active sites and unique functional groups. Hence, it is predicted that co-doped sulfonated carbon
366 dots and CS on the biochar could improve adsorption performance. After introducing CS into *h*-
367 CD/MCSB, the presence of -NH₂ as an active group and electron-withdrawing groups can create
368 a high delocalization energy in the functional groups of CS decorated on *h*-CDs/MCSB. As a
369 result, the hydrogen atoms of the anthracene ring bond with oxygen atoms of *h*-CDs/MCSB
370 through polarization-assisted H-bond (or σ -bond cooperative) (Fig. 5c)(Ahmed et al. 2017;
371 Prasannamedha et al. 2021). Moreover, multiple functional groups polarization-assisted H-bond,
372 π -bond, and electrostatic interaction might also enhance the anthracene adsorption.

373 The presence of -CH₃ groups in CS, can lead to the overlap of an orbital of adjacent C--H
374 σ bond with an empty p orbital of adjacent carbon. The delocalization of electrons from a sigma

375 bond orbital to an empty p orbital can decrease the charge density on the sp^2 carbon and thereby
 376 can generate bonds with anthracene molecules (Fan et al. 2021; Lopes and Astruc 2021). This
 377 overlapping owing to the delocalization of electrons between a sigma bond orbital with an empty
 378 orbital on the adjacent carbon is called hyperconjugation (Kirmizakis et al. 2020; Hao et al. 2021)
 379 (Fig. 6a and 6b). The interaction is mainly based on the difference of energy between the C–H
 380 bonding (σ) molecular orbital on one carbon of *h*-CDs/MCSB and the C-H antibonding (σ^*)
 381 molecular orbital on the other carbon of anthracene, resulting in a partial moving of
 382 electrons in the filled bonding molecular orbital into unoccupied antibonding molecular orbital.

383



384

385

386

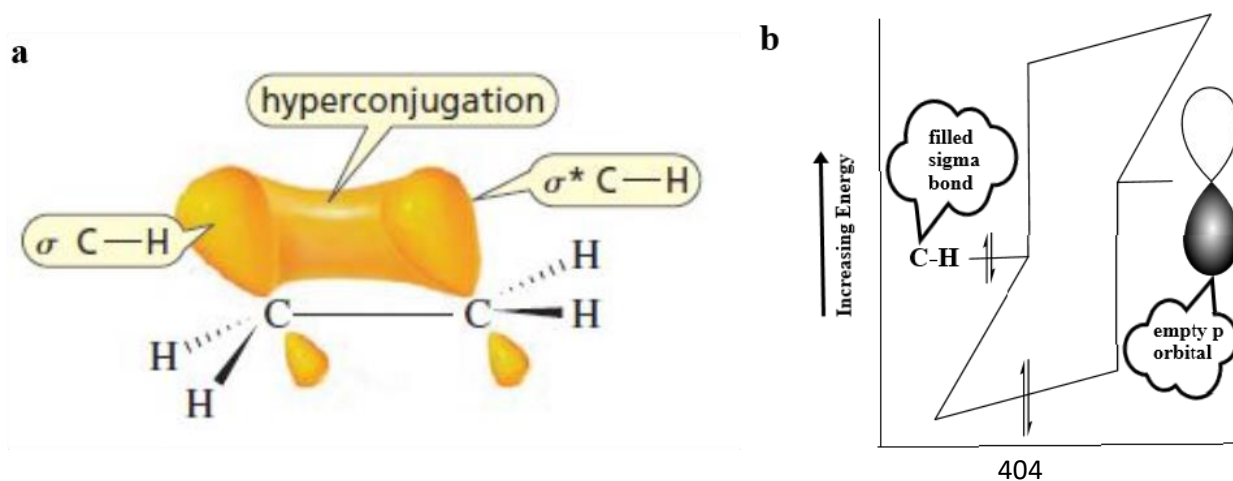
387

388

389 **Fig. 5: Structural details of the complex of anthracene with active sites of CDs/MCSB (a and**
 390 **b); and *h*-CDs/MCSB (c) (point: with locating hydrogen atoms between the two**
 391 **electronegative atoms (oxygen and nitrogen), the strongest hydrogen bond is formed. The**
 392 **presence of polar and hydrogen bonds simultaneously leads to stronger and stabilization of**
 393 **adsorption bonds effectively through more polarizability of functional groups derived by CS**
 394 **addition to the adsorbent).**

395 The stabilization was achieved by the overlap of a filled C-H sigma bond orbital with a
 396 vacant p orbital (Zhao et al. 2021; Lin, Wu, and Mo 2019). As a result, the interaction energy of
 397 *h*-CDs/MCSB with anthracene molecules decreased to -42.25 eV. Moreover, the Mulliken charges
 398 of oxygen atom in the *h*-CDs/MCSB was lower than the CDs/MCSB hybrid alone (-0.522 against
 399 -0.582), suggesting that more polarized functional groups in *h*-CDs/MCSB than that of
 400 CDs/MCSB hybrid (Table S2). At the same time, anthracene molecules and *h*-CDs/MCSB could
 401 be considered as H- donor and H-acceptor, respectively. In summary, in an aqueous solution, the
 402 CDs/MCSB is less stable than *h*-CDs/MCSB.

403



405 **Fig. 6: a) stabilization induced by delocalization of electrons between functional groups and**
 406 **anthracene molecules; and b) a related molecular orbital diagram of hyperconjugation.**

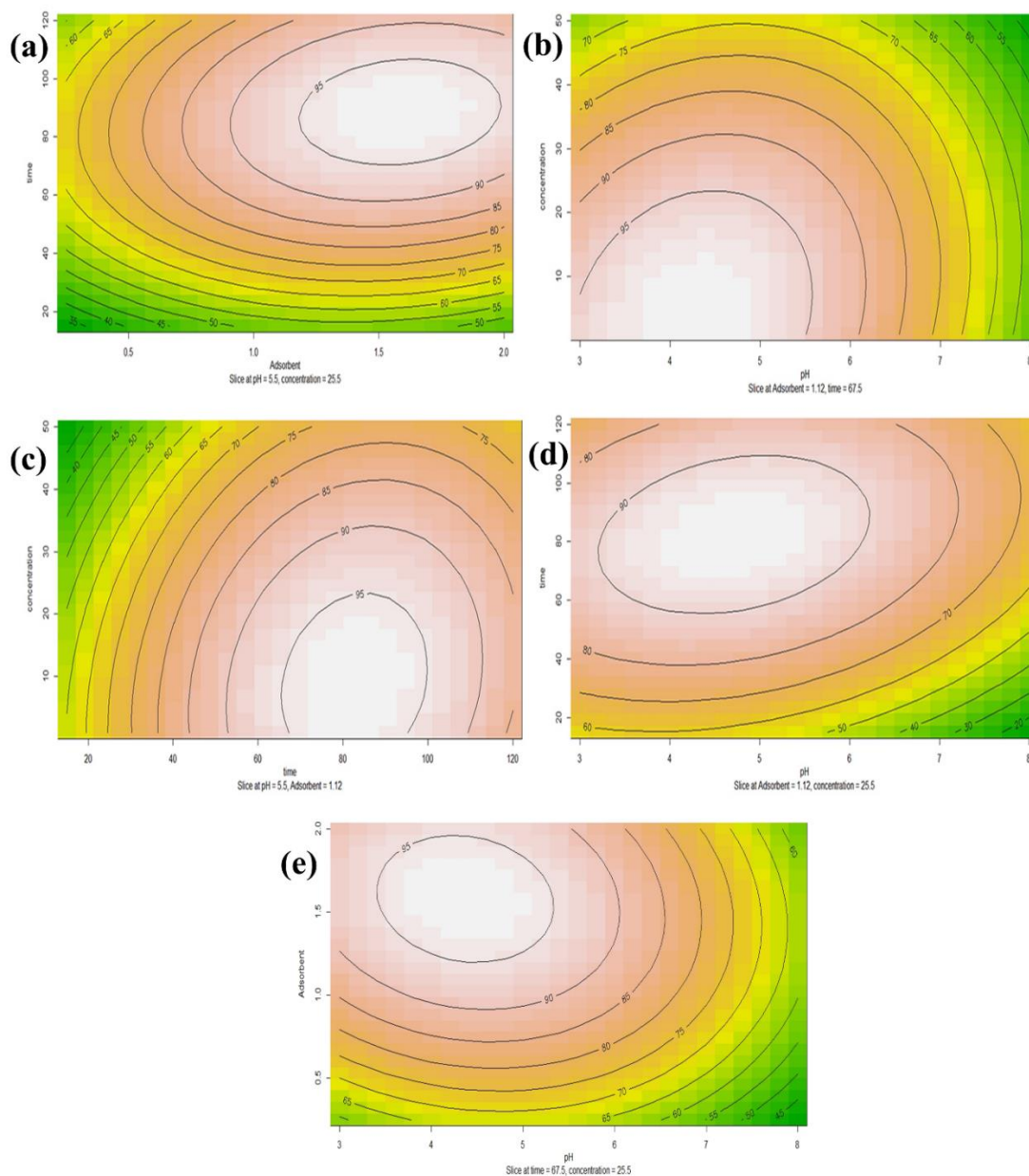
407 3.3. The effects of experimental conditions on the adsorption process

408 Due to the presence of anthracene in various environmental media with varying pH, it was critical
 409 to understand the adsorption behavior of anthracene onto *h*-CDs/MCSB over a chemically relevant
 410 pH range. The initial anthracene concentration from 1 to 50 mg L⁻¹ was investigated to achieve
 411 optimum adsorption of anthracene onto the *h*-CDs/MCSB, which attained the highest removal
 412 efficiency of 94% at an initial concentration of 10 mg L⁻¹ (Fig. S3). It was found that the acid
 413 activation of carbonized biochar and merging with CS were a way to improve and create various
 414 active sites (or active groups) and thereby enhance adsorption capacity for the treatment of
 415 anthracene. The good performance of modified chitosan with *h*-CDs/MCSB for anthracene

416 removal could be related to the incorporation of plentiful functional groups as active sites that
417 leads to operates adsorption process under a wide range of pH condition.

418 To optimize the influenced parameters on anthracene adsorption capacity, Analysis of
419 variance (ANOVA) and Response Surface Methodology (RSM) were performed and fitted
420 significantly to the experiment data. As shown in Table S4, the higher value of F could be
421 interpreted by the regression equation, and the p-values less than 0.001 are regarded to be
422 statistically significant. According to Table S4, all p-values of experiment parameters are less than
423 0.001 except for initial concentration, indicating great influences of the main parameters on
424 anthracene adsorption capacity. Fig. 7 (7a, 7b, 7c, 7d, and 7e) exhibits the 2D surface plots of
425 collective interaction effects of the independent variables on anthracene adsorption capacity that
426 are presented as a function of two factors by holding other factors at fixed levels.

427 As exhibited in Fig. 8a, the anthracene sorption by *h*-CDs/MCSB decreased as the pH of
428 the anthracene solution increased from 5 to 8 with the highest (q_e) value of 8.78 mg g⁻¹ achieved
429 at pH 5 and 10 mg L⁻¹ initial anthracene concentration. The q_e of *h*-CDs/MCSB slightly decreased
430 when the pH increased to > 7, likely due to the deprotonation of oxygen-containing surface
431 functional groups (e.g., ketone, carboxyl, ether, and lactone groups), free -NH₂, and -OH active
432 groups that increased at high pH (Ren et al. 2022; Li, Yang, et al. 2022). The suggested reason for
433 this can be ascribed to less tendency of the interaction of functional groups in *h*-CDs/MCSB with
434 the π -electron cloud existed in anthracene due to the negatively charged *h*-CDs/MCSB surface that
435 is one of the main mechanisms in the adsorption of anthracene (Brown et al. 2013). Due to multi-
436 functional and plentiful functional, active groups of *h*-CDs/MCSB, effective adsorption of
437 anthracene spanned across a wide range of pH.



438
 439 **Fig. 7: 2D surface plot for the interactive effect of variable parameters of anthracene**
 440 **adsorption by CS decorated *h*-CDs/MCSB, (a) Reaction time versus *h*-CDs/MCSB dose, (b)**
 441 **Anthracene concentration versus pH, (c) Anthracene concentration versus reaction time, (d)**
 442 **Reaction time versus pH, and (e) *h*-CDs/MCSB dose versus pH.**

443 At lower pH, active groups of *h*-CDs/MCSB such as carboxyl, carboxylic, quinine, and
 444 lactone could be formed (Bruce 2006). These active groups promote the adsorption of PAHs. Fig.
 445 8a shows the percentage of anthracene adsorption initially increased from 85% at pH 3 to 87% at
 446 pH 5. However, beyond the equilibrium pH (pH 5), the anthracene adsorption efficiency slightly

447 decreased to 82% (at pH 7), which might be due to the decline of electrostatic charge potential
448 between *h*-CDs/MCSB and anthracene molecule (Wade and Simek 2017). Previous studies also
449 reported higher adsorption of anthracene at lower ranges of pH, particularly acidic pH. For
450 instance, Zango et al. reported the highest adsorption capacities of anthracene at pH 2 by two
451 adsorbents, NH₂-MIL-88(Fe) and MIL-88 (Fe)(Zango et al. 2019). Another study on vehicular
452 tire-based activated carbon for anthracene removal reported the reduction of anthracene by ~90%
453 at pH 2(Gupta 2018). In another study, anthracene adsorbed on β -cyclodextrin functionalized
454 magnetite hydrochar at a wide range of pH, although the adsorption capacity was low and
455 insignificant (by up to ~50%) (Qu et al. 2021).

456 The low adsorption capacity of anthracene by CS is related to poor mechanical strength,
457 weak stability and solubility in acid, low hydrophilic, and low surface area(Usman et al. 2021).
458 These challenges could be resolved by combining CDs/MCSB and modified CS into a multi-
459 functional adsorbent (*h*-CDs/MCSB). The enriched active groups of *h*-CDs/MCSB permit the
460 preservation of hydroxyl, carboxyl, and other functional groups on the surface of *h*-CDs/MCSB
461 through covalent bonding to CS (the bonding mainly taking place through the -NH₂ and -OH
462 groups) at acidic pH. The benefit of modified *h*-CDs/MCSB was the applicability of the adsorbent
463 for anthracene removal with a wide pH range of solution. The pH of 5 was chosen for further
464 experiments and parameter optimization.

465 Reaction time as another parameter influencing anthracene adsorption by *h*-CDs/MCSB
466 was studied (Fig. 8b). The equilibrium adsorption time of anthracene on *h*-CDs/MCSB was ~90
467 min, achieving a high removal efficiency (~92 %) and q_e of 9.24 mg g⁻¹. Interestingly, the fast
468 adsorption of anthracene (Table 1) suggests *h*-CDs/MCSB as a promising biogenic adsorbent for
469 the effective remediation of aqueous phase anthracene. The batch mode adsorption experiment
470 showed rapid adsorption of anthracene within the first 60 min, and then it proceeded steadily state
471 until equilibrium was achieved might be due to the greater availability of active binding sites and
472 incorporation of multifarious functional groups and preserving active groups by *h*-CDs/MCSB
473 (Bao et al. 2021). Moreover, (Kamińska et al. 2019) reported that the rapid adsorption of
474 anthracene might be due to the covalent bonding between -NH₂, and -OH chelating
475 sites and some active functional groups, including carboxyl, amino, sulfonic groups (binding
476 sites). The adsorption performance of *h*-CDs/MCSB was superior compared to those of other

477 adsorbents (Table 1), making it a promising adsorbent for the removal of PAH, particularly
 478 anthracene.

479

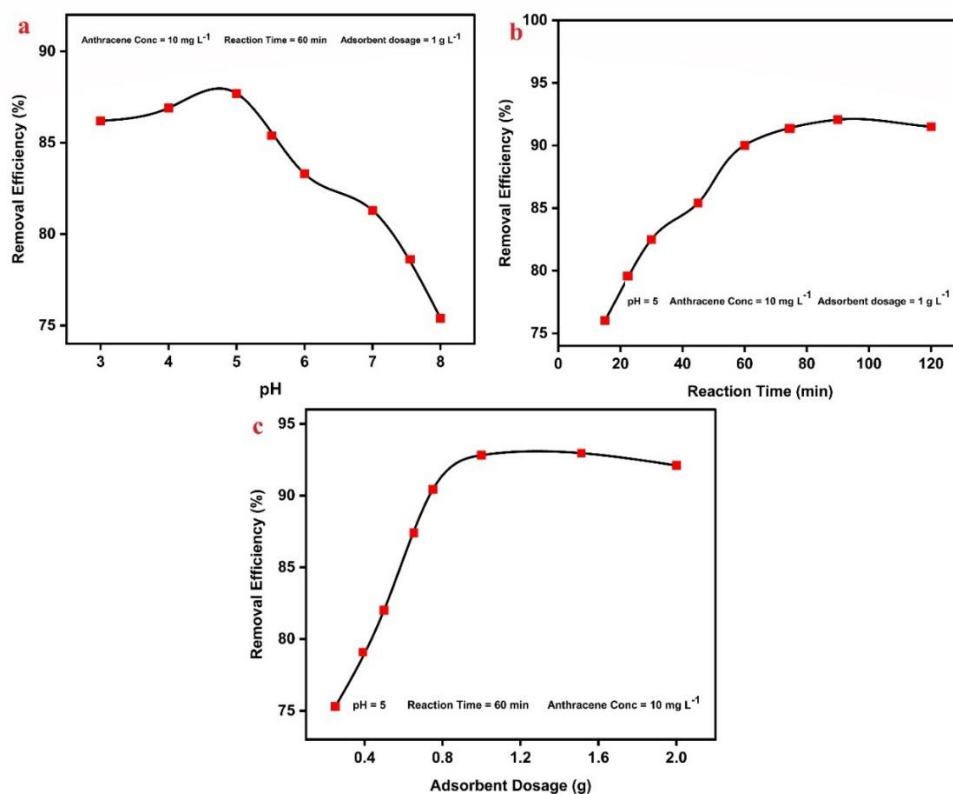
480

481 **Table 1. Comparisons of various materials carried out for the adsorption of anthracene**

Materials	Equilibrium time (mins)	Initial concentration (mg L ⁻¹)	Dosage (g L ⁻¹)	Optimum pH	% Removal	Q_{max} (mg g ⁻¹)	Ref.
Waste vehicular tyres (VTAC)	75	40	0.8	2	99	142.24	(Gupta 2018)
β -Cyclodextrin functionalized magnetic hydrochar	80	30	0.5	5.5	-	60.27	(Qu et al. 2021)
Mixed-MIL-88(Fe)	25	4	0.5	6	95	23	(Zango et al. 2019)
NH2-MIL-88(Fe)	25	4	0.5	6	92	22.2	(Zango et al. 2019)
MIL-88(Fe)	25	4	0.5	6	98	23.6	(Zango et al. 2019)
MgO-carbon composite	60	25	0.6	5	96	17.07	(Kumar et al. 2019)
Activated carbon	30	4	0.3	-	-	8.35	(Saad et al. 2014)
Granular activated carbon	400	10	0.3	-	-	14.6	(Valderrama et al. 2008)
Non-imprinted silica aerogel	240	2.4	0.1	-	38	-	(Saad et al. 2020)
Hal-CNT composite	30	1	0.25	-	-	0.45	(Kamińska et al. 2019)
NGO/SA/PVA microspheres	1440	0.5	0.05	-	65	4.63	(Song et al. 2021)
Fe ₃ O ₄ /MIL-101	60	4	-	6	95	12.7	(Tirado-Guizar et al. 2020)
CS-decorated <i>h</i> -CDs/MCSB	60	10	1	5	>95	49.26	Present study

482

483 Resource recovery and conservation of materials in the removal process can lead the
 484 remediation technologies. Therefore, the required dose to achieve the optimum removal was
 485 investigated along with other variable factors. A wide range of *h*-CDs/MCSB dose from 0.25 to 2
 486 g at pH 5 with 10 mg L⁻¹ initial anthracene concentration was examined. The best removal
 487 efficiency was achieved at the adsorbent dosage of 1 g (Fig. 8c). Due to the very low surface area
 488 and weak stability of active sites for CS, adding *h*-CDs/MCSB to CS could increase surface area
 489 and preserve active sites of CS surface. Here, *h*-CDs/MCSB composite exhibits a structure with
 490 favorable strength and porous structure. As shown in Fig. 8c, the increase in dose of adsorbent
 491 enhanced the active binding sites available on the adsorbent surface for the adsorption of
 492 anthracene with 1 g of adsorbent. Moreover, beyond the optimum dose (1 g L⁻¹), the adsorption
 493 efficiency of anthracene did not change substantially due to the high dosage of *h*-CDs/MCSB
 494 could lead to aggregation of adsorbent hybrid (Singh et al. 2022). Moreover, FTIR and Raman
 495 studies indicated the *h*-CDs/MCSB to be a multi- and variable active site that could reach a higher
 496 and faster adsorption performance than CDs/MCSB without CS.



497
 498 **Fig. 8: The impacts of process variables on the adsorption process by *h*-CDs/MCSB; (a) pH,**
 499 **(b) reaction time, and (c) adsorbent dosage.**

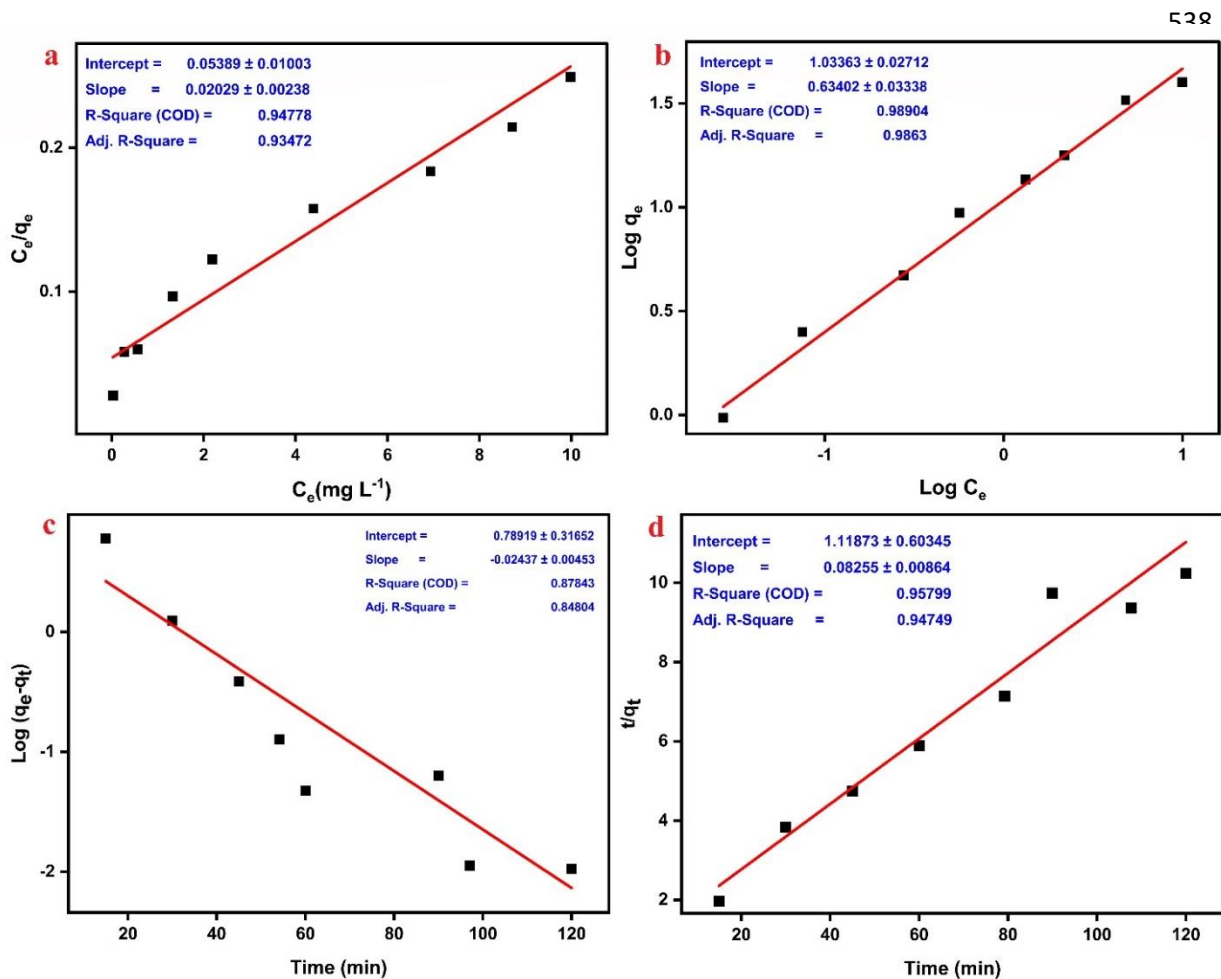
500 3.4. Isotherms and kinetics of adsorption

501 The adsorption of anthracene onto *h*-CDs/MCSB was modeled by Langmuir and Freundlich
502 expressions. Depicted in Fig. 9a and 9b and Table S5, the Langmuir isotherm demonstrates a high
503 correlation coefficient (R^2) than the Freundlich isotherm, indicating the adsorption process of
504 anthracene over *h*-CDs/MCSB is more agreeable with Langmuir model. Moreover, the close value
505 of a maximum of experimental adsorption capacity ($Q_{\max, \text{exp}}$) to the theoretical (Langmuir)
506 equilibrium of adsorption capacity than that of Freundlich maximum of adsorption capacity
507 (theoretical and experimental), was demonstrated that the Langmuir model is more appropriate for
508 explaining the equilibrium data of *h*-CDs/MCSB. The better agreement with Langmuir model
509 suggests that the anthracene adsorption on the *h*-CDs/MCSB was monolayer coverage. Moreover,
510 the adsorption energetics (n) constant was lower than 1, indicating favorability of anthracene
511 adsorption process (Shaikh, Chakraborty, et al. 2022). The R_L parameter (Langmuir constant)
512 calculated from the Langmuir model (Fig. S4), conveyed the favorability of the adsorption process.
513 We proposed that the modification and stabilization of functional groups of biochar surface with
514 chitosan enhanced the homogeneity of the *h*-CDs/MCSB surface, providing a uniform distribution
515 of finite and multifarious active groups on the adsorbent and monolayer coverage of anthracene
516 on the *h*-CDs/MCSB. The isotherms interpretation was consistent with the monolayer coverage of
517 anthracene observed by BET and SEM images.

518 Generally, adsorption is considered to be a complex synergistic phenomenon of manifold
519 stages involving multiple mechanisms, including multiple scales and species (of the adsorbate)
520 (Kundu and Gupta 2007). The adsorption results yield the following deductions: (a) monolayer
521 anthracene adsorption onto *h*-CDs/MCSB, (b) anthracene adsorption occurred on homogeneous *h*-
522 CDs/MCSB, (c) electrostatic interaction between *h*-CDs/MCSB, and (d) significant improvement
523 of anthracene adsorption was achieved using *h*-CDs/MCSB.

524 The kinetics of adsorption of anthracene onto *h*-CDs/MCSB was characterized by the
525 pseudo-1st order and pseudo-2nd order models. As shown in Fig. 9c and 9d, and Table S5, the
526 pseudo-2nd order is a better fit with the experimental data. Generally, the four main stages are
527 suggested to be involved in the adsorption of anthracene by *h*-CDs/MCSB. To begin with, the
528 adsorption process was started with the mass transfer of anthracene molecules and completely
529 dissolved in solution. In addition, the process was continued with the slow diffusion of anthracene

530 molecules towards the surface of the *h*-CDs/MCSB (film diffusion). Furthermore, the movement
 531 of anthracene molecules from the surface into the porous of *h*-CDs/MCSB (intraparticle diffusion).
 532 Finally, the binding active moieties of anthracene with active sites of the *h*-CDs/MCSB. As the
 533 micropores and mesopores contribute the majority of *h*-CDs/MCSB, so the rapid transport of
 534 anthracene ions through the channels of micro/mesopores can decrease the effects of film and
 535 intraparticle diffusion (Shaikh, Kumar, Chakraborty, Islam, et al. 2022). Also, the adsorption
 536 process of anthracene molecules on *h*-CDs/MCSB was chemisorption rather than diffusion
 537 controlled (Shaikh, Kumar, Chakraborty, Naushad, et al. 2022).



543 **Fig. 9: The plotted isotherms and Kinetics of *h*-CDs/MCSB**

544

545 The overall kinetics model results of anthracene adsorption onto the *h*-CDs/MCSB suggest
 546 (a) chemisorption dominated adsorption mechanism, where a significant role was played by ion-

547 exchange, (b) rate of anthracene uptake was directly dependent on the square of remaining
 548 anthracene concentration in solution, where surface adsorption was one of the major dominating
 549 factors, and (c) a complex anthracene adsorption mechanism including surface adsorption, π - π
 550 staking, H-bonding, and electrostatic attraction.

551 **3.5. Thermodynamic study**

552 The adsorption process was further investigated in terms of the effect of temperature (298.15,
 553 308.15, and 318.15 K). The related parameters, such as enthalpy (ΔH°), entropy (ΔS°), and Gibbs
 554 free energy (ΔG°), were calculated by these following equations to understand adsorption
 555 mechanisms (Shaikh, Kumar, Chakraborty, Islam, et al. 2022; Shaikh, Islam, and Chakraborty
 556 2021):

$$557 \quad \Delta G^\circ = -RT \ln K \quad (8)$$

$$558 \quad \ln K = -\frac{\Delta G^\circ}{RT} = -\frac{\Delta H^\circ}{RT} + \frac{\Delta S^\circ}{R} \quad (9)$$

559 Where K and R (8.314 J mol⁻¹ K⁻¹) are the adsorption equilibrium constant and universal gas
 560 constant, respectively.

561 The vant Hoff curve for the anthracene sorption on *h*-CDs/MCSB is shown in Fig. S5, and
 562 the related calculated thermodynamic parameters are presented in Table S6. The negative value of
 563 ΔG° indicates that the anthracene adsorption process was spontaneous and thermodynamically
 564 favorable and exothermic (Hassan et al. 2022).

565

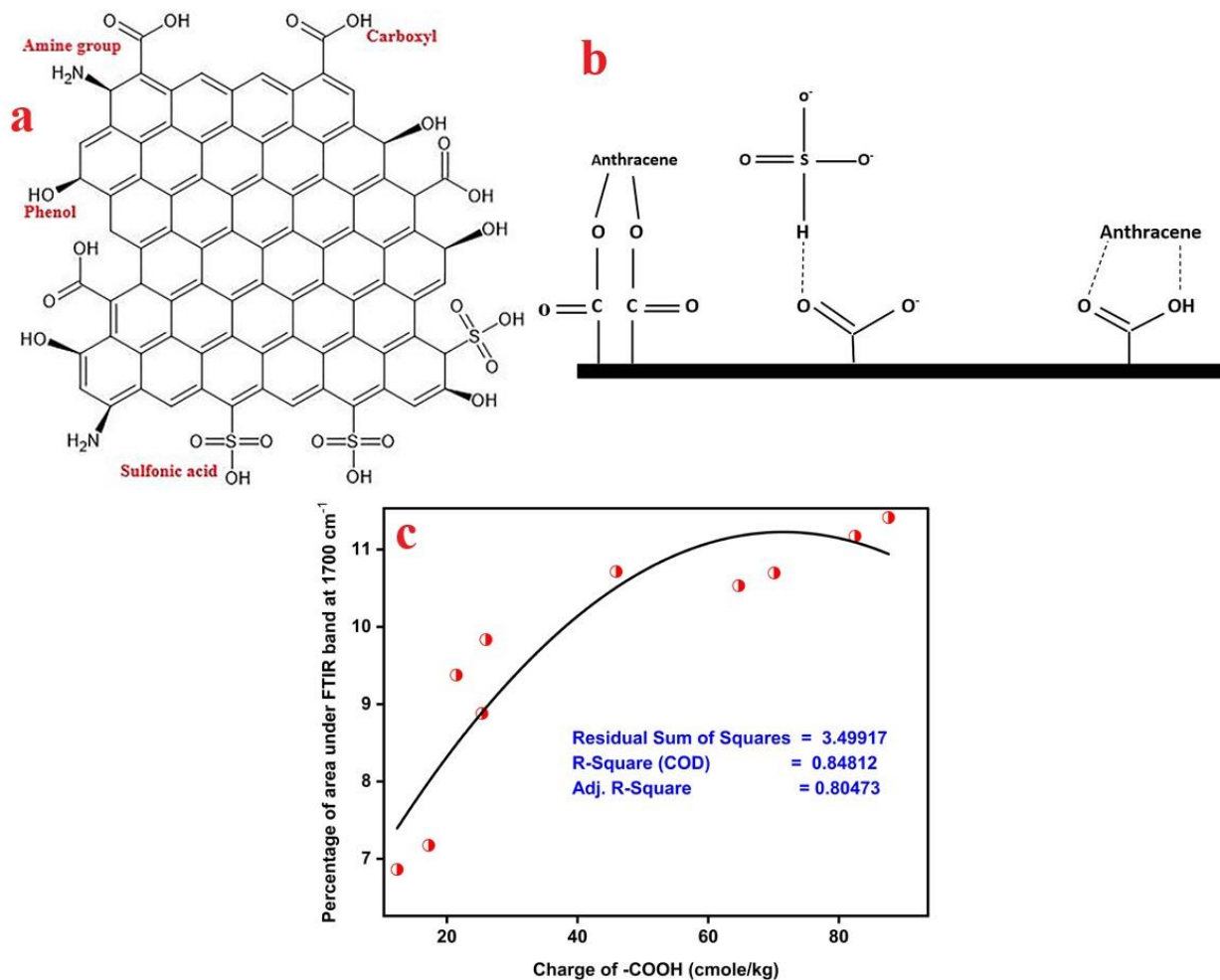
566 **3.6. Mechanistic insights into anthracene removal**

567 Activation and modification of the biochar by the sulfonating process provided a homogeneous
 568 dispersion of CDs onto MCSB. Therefore, oxyanion groups (e.g., sulfonic and carboxylic acid
 569 groups) bonded with CDs in the biochar matrix (Table S1). Further, through hybridizing
 570 CDs/MCSB with CS (*h*-CDs/MCSB), the methylene group in CH₂OH, methine group in the
 571 pyranose ring, and -NH₂ groups of CS were formed and remained on *h*-CDs/MCSB (Fig. 10a).
 572 These multifarious and multitudinous active groups on *h*-CDs/MCSB could play a critical role in
 573 the interaction between *h*-CDs/MCSB and anthracene in aqueous solution. It is believed that the

574 high polarity of the synthesized composite drives the anthracene adsorption due to polar functional
575 groups and NH_2 protonation of the polymeric chain. This resulted in an excellent affinity for
576 intra/inter molecular hydrogen bonding between *h*-CDs/MCSB and anthracene, thus enhancing the
577 adsorption performance (Hino, Matsuo, and Hayashi 2022). For example, protonation of NH_2
578 under isotropic pH, fosters a large number of cationic sites, which can serve as complexation sites
579 for anthracene and other potential co-contaminants in aqueous solutions.

580 The generation of high polarity on the surface of *h*-CDs/MCSB with CS introduction, the
581 *h*-CDs/MCSB is provided the affording good affinity for generating intra-molecular and
582 intermolecular hydrogen bonding (H-bond donating/accepting). The C-H bonds in anthracene and
583 O or N in the *h*-CDs/MCSB can serve as H-bond donors and acceptors, respectively. Moreover,
584 both the carboxylic and phenolic hydroxyls in the *h*-CDs/MCSB can serve as both H-bond donors
585 and acceptors. Under unfavorable pH for $-\text{NH}_2$ protonation, the oxygen-containing groups (e.g., -
586 SO_3H and $-\text{COOH}$) act as H-bond accepting sites to generate H-bonds with H-bond donors (Fig.
587 10b). The carboxylic groups on the *h*-CDs/MCSB could stabilize the negatively charged oxygen
588 due to inductive electron withdrawal and delocalized electrons, suggesting the establishment of
589 the active groups on the *h*-CDs/MCSB as well as potential to reuse the adsorbent (Ajani et al.
590 2022).

591 Another mechanism involved in the adsorption process could be electrostatic attraction or
592 repulsion between *h*-CDs/MCSB and anthracene that was derived from the surface charge of *h*-
593 CDs/MCSB (Wiśniowska and Włodarczyk-Makuła 2022). The sulfonated and oxygen-containing
594 groups (such as aliphatic surface) could be ascribed to generate surface charges of *h*-CDs/MCSB,
595 confirmed by a linear relationship between surface charge of $-\text{COOH}$ and determined from FTIR
596 band at 1700 cm^{-1} of *h*-CDs/MCSB (Fig. 10c).



597
 598 **Figure 10. (a and b) the adsorption mechanisms of Anthracene on CS adorned *h*-CDs/MCSB,**
 599 **and (c) the obtained sulfonated and oxygen-containing groups CS adorned *h*-CDs/MCSB**

600

601

602

603

604

605

606 **4. Conclusions**

607 This study showed that the modification of biochar is necessary for the effective removal of
608 anthracene from an aqueous solution. This work provides a new insight into interactions between
609 benzene rings of anthracene and π -polarized hydrogen bonds induced by CS addition besides rich-
610 functional groups of *h*-CDs/MCSB. The CDs-derived acid treatment of coconut shell biochar was
611 also functionalized by sulfonic and carboxylic groups and could be served as additional active sites
612 on the hybrid adsorbent. The complex generated by polarized functional groups induced CS, and
613 aromatically rich-functionalized CDs derived coconut shell biochar could serve as an H-acceptor
614 source for available for hydrogen bonding. Moreover, the induced polarizability of the functional
615 groups and increasing electron delocalization could be responsible for improving the sorption
616 ability of π -electron delocalized stable benzene rings of anthracene. The higher capacity and fast
617 removal of anthracene were achieved by *h*-CDs/MCSB adsorbent, with 49.26 mg g⁻¹ at 60 min.
618 The suitability of the Langmuir isotherm and pseudo-second order kinetic model for describing
619 the adsorption data suggest monolayer adsorption of anthracene on CS adorned *h*-CDs/MCSB and
620 chemisorption as a rate-determining step, respectively. The CDs functionalized active functional
621 groups, and their dispersion over porous micro/mesoporous structures of carbon network was
622 confirmed. It is worth noting that the rich-functional groups (acidic and oxygen-containing groups)
623 were anchored on both the coconut shell biochar as well as on the CDs. The outcomes of this work
624 are significant as the proposed methodology for the CDs can be used for other carbon-based
625 adsorbents with a great potential for water/wastewater treatment applications, in particular,
626 emerging and persistent organic pollutants with similar properties as PAHs, especially anthracene.

627

628 **Acknowledgments**

629 The financial support of this research was from the Water and Wastewater Research Center, Water
630 Research Institute (WRI), Tehran, Iran.

631

632

633 **5. References**

- 634 Adeola, Adedapo O, and Patricia BC Forbes. 2021. 'Advances in water treatment technologies for
635 removal of polycyclic aromatic hydrocarbons: Existing concepts, emerging trends, and future
636 prospects', *Water Environment Research*, 93: 343-59.
- 637 Ahmed, MJ, BH Hameed, and EH Hummadi. 2020. 'Review on recent progress in chitosan/chitin-
638 carbonaceous material composites for the adsorption of water pollutants', *Carbohydrate
639 Polymers*, 247: 116690.
- 640 Ahmed, Mohammad Boshir, John L Zhou, Huu Hao Ngo, Wenshan Guo, Md Abu Hasan Johir, and
641 Kireesan Sornalingam. 2017. 'Single and competitive sorption properties and mechanism of
642 functionalized biochar for removing sulfonamide antibiotics from water', *Chemical Engineering
643 Journal*, 311: 348-58.
- 644 Ajani, Ayobami Olu, Olufunmilayo Abiola Aworanti, Jimoh Olugbenga Hamed, Samuel Enahoro Agarry,
645 and Oladipo Olaosebikan Ogunleye. 2022. 'Kinetic Modelling of Adsorptive Biodegradation of
646 Anthracene onto Activated Carbon', *Appl. J. Envir. Eng. Sci*, 8: 8-1 (2022) 95-111.
- 647 Amorini, Mattia, Nicolò Riboni, Lucia Pesenti, Valentina Antonia Dini, Alessandro Pedrini, Chiara
648 Massera, Chiara Gualandi, Federica Bianchi, Roberta Pinalli, and Enrico Dalcanale. 2022.
649 'Reusable Cavitand-Based Electrospun Membranes for the Removal of Polycyclic Aromatic
650 Hydrocarbons from Water', *Small*, 18: 2104946.
- 651 Baharum, Nor Atikah, Hanisah Mohmad Nasir, Mohd Yusoff Ishak, Noorain Mohd Isa, Mohd Ali Hassan,
652 and Ahmad Zaharin Aris. 2020. 'Highly efficient removal of diazinon pesticide from aqueous
653 solutions by using coconut shell-modified biochar', *Arabian Journal of Chemistry*, 13: 6106-21.
- 654 Bao, Zhen-Zong, Zhi-Feng Chen, Si-Qi Lu, Guangzhao Wang, Zenghua Qi, and Zongwei Cai. 2021. 'Effects
655 of hydroxyl group content on adsorption and desorption of anthracene and anthrol by polyvinyl
656 chloride microplastics', *Science of the Total Environment*, 790: 148077.
- 657 Brown, William H, Brent L Iverson, Eric Anslyn, and Christopher S Foote. 2013. *Organic chemistry*
658 (Cengage Learning).
- 659 Bruice, Paula Yurkanis. 2006. *Essential organic chemistry* (Pearson Education Upper Saddle River).
- 660 Chen, Hanbo, Yurong Gao, Ali El-Naggar, Nabeel Khan Niazi, Chenghua Sun, Sabry M Shaheen, Deyi Hou,
661 Xing Yang, Zhiyuan Tang, and Zhongzhen Liu. 2022. 'Enhanced sorption of trivalent antimony by
662 chitosan-loaded biochar in aqueous solutions: Characterization, performance and mechanisms',
663 *Journal of Hazardous materials*, 425: 127971.
- 664 Chen, Shanshan, Amelia-Elena Rotaru, Pravin Malla Shrestha, Nikhil S Malvankar, Fanghua Liu, Wei Fan,
665 Kelly P Nevin, and Derek R Lovley. 2014. 'Promoting interspecies electron transfer with biochar',
666 *Sci. Rep*, 4: 1-7.
- 667 Chen, Wei-Hsin, Anh Tuan Hoang, Sandro Nižetić, Ashok Pandey, Chin Kui Cheng, Rafael Luque, Hwai
668 Chyuan Ong, Sabu Thomas, and Xuan Phuong Nguyen. 2022. 'Biomass-derived biochar: From
669 production to application in removing heavy metal-contaminated water', *Process Safety and
670 Environment Protection*, 160: 704-33.
- 671 da Silva Medeiros, Deborah Cristina Crominski, Pamela Chelme-Ayala, Chelsea Benally, Bader S Al-Anzi,
672 and Mohamed Gamal El-Din. 2022. 'Review on carbon-based adsorbents from organic
673 feedstocks for removal of organic contaminants from oil and gas industry process water:
674 Production, adsorption performance and research gaps', *Journal of Environmental Management*,
675 320: 115739.
- 676 Dai, Lichun, Qian Lu, Haiqin Zhou, Fei Shen, Zhengang Liu, Wenkun Zhu, and Huagang Huang. 2021.
677 'Tuning oxygenated functional groups on biochar for water pollution control: A critical review',
678 *Journal of Hazardous materials*, 420: 126547.

- 679 Dai, Yingjie, Naixin Zhang, Chuanming Xing, Qingxia Cui, and Qiya Sun. 2019. 'The adsorption,
680 regeneration and engineering applications of biochar for removal organic pollutants: a review',
681 *Chemosphere*, 223: 12-27.
- 682 Dehghani, Mohammad Hadi, Daryoush Sanaei, Imran Ali, and Amit Bhatnagar. 2016. 'Removal of
683 chromium (VI) from aqueous solution using treated waste newspaper as a low-cost adsorbent:
684 kinetic modeling and isotherm studies', *Journal of Molecular Liquids*, 215: 671-79.
- 685 Dehghani, Mohammad Hadi, Mohammad Sarmadi, Mohammad Reza Alipour, Daryoush Sanaei, Hamid
686 Abdolmaleki, Shilpi Agarwal, and Vinod Kumar Gupta. 2019. 'Investigating the equilibrium and
687 adsorption kinetics for the removal of Ni (II) ions from aqueous solutions using adsorbents
688 prepared from the modified waste newspapers: A low-cost and available adsorbent',
689 *Microchemical Journal*, 146: 1043-53.
- 690 Ding, Liping, and Yu Fang. 2010. 'Chemically assembled monolayers of fluorophores as chemical sensing
691 materials', *Chemical Society Reviews*, 39: 4258-73.
- 692 Fan, Yuxing, Liangliang Huang, Ligui Wu, Chuanting Zhang, Shuhui Zhu, Xiaoyu Xiao, Mi Li, and Xiaoming
693 Zou. 2021. 'Adsorption of sulfonamides on biochars derived from waste residues and its
694 mechanism', *Journal of Hazardous materials*, 406: 124291.
- 695 Feng, Zhaoxuan, Karin H Adolfsson, Yanan Xu, Haiqiu Fang, Minna Hakkarainen, and Mingbo Wu. 2021.
696 'Carbon dot/polymer nanocomposites: From green synthesis to energy, environmental and
697 biomedical applications', *SM&T*, 29: e00304.
- 698 Gholami, Peyman, Alireza Khataee, Amit Bhatnagar, and Behrouz Vahid. 2021. 'Synthesis of N-doped
699 magnetic WO₃-x@ Mesoporous carbon using a diatom template and plasma modification:
700 visible-light-Driven Photocatalytic activities', *ACS Applied Materials & Interfaces*, 13: 13072-86.
- 701 Gong, Heyang, Yuefen Li, and Shujie Li. 2021. 'Effects of the interaction between biochar and nutrients
702 on soil organic carbon sequestration in soda saline-alkali grassland: A review', *Glob Ecol Conserv*,
703 26: e01449.
- 704 González-González, Reyna Berenice, Lucy Teresa González, Marc Madou, César Leyva-Porras, Sergio
705 Omar Martinez-Chapa, and Alberto Mendoza. 2022. 'Synthesis, Purification, and
706 Characterization of Carbon Dots from Non-Activated and Activated Pyrolytic Carbon Black',
707 *Nanomaterials*, 12: 298.
- 708 Gupta, Himanshu. 2018. 'Anthracene removal from water onto activated carbon derived from vehicular
709 tyre', *Separation Science and Technology*, 53: 613-25.
- 710 Gurav, Ranjit, Shashi Kant Bhatia, Tae-Rim Choi, Yong-Keun Choi, Hyun Joong Kim, Hun-Suk Song, Sol Lee
711 Park, Hye Soo Lee, Sun Mi Lee, and Kwon-Young Choi. 2021. 'Adsorptive removal of crude
712 petroleum oil from water using floating pinewood biochar decorated with coconut oil-derived
713 fatty acids', *Science of the Total Environment*, 781: 146636.
- 714 Hao, Na, Junnan Cao, Jianshe Ye, Chi Zhang, Chen Li, and Bate Bate. 2021. 'Content and morphology of
715 lead remediated by activated carbon and biochar: a spectral induced polarization study', *Journal
716 of Hazardous materials*, 411: 124605.
- 717 Hashmi, Zubair, Abdul Sattar Jatoti, Saad Nadeem, Amna Anjum, Syed Mazhar Imam, and Haroon Jangda.
718 2022. 'Comparative analysis of conventional to biomass-derived adsorbent for wastewater
719 treatment: a review', *Biomass Conversion and Biorefinery*: 1-32.
- 720 Hassan, Ahmed Abdi, Abdulkadir Tanimu, Saheed A Ganiyu, Ibrahim Y Yaagoob, and Khalid Alhooshani.
721 2022. 'Selective removal of Cd (II), As (III), Pb (II) and Cr (III) ions from water resources using
722 novel 2-anthracene ammonium-based magnetic ionic liquids', *Arabian Journal of Chemistry*, 15:
723 104136.
- 724 Hino, Yuto, Takumi Matsuo, and Shotaro Hayashi. 2022. 'Structural phase transitions in anthracene
725 crystals', *ChemPlusChem*, 87: e202200157.

- 726 Huang, Xixian, Yunguo Liu, Shaobo Liu, Xiaofei Tan, Yang Ding, Guangming Zeng, Yaoyu Zhou, Mingming
 727 Zhang, Shufan Wang, and Bohong Zheng. 2016. 'Effective removal of Cr (VI) using β -
 728 cyclodextrin–chitosan modified biochars with adsorption/reduction bifunctional roles', *RSC Adv*,
 729 6: 94-104.
- 730 Imam, Arfin, Sunil Kumar Suman, Raghuvir Singh, Bhanu Prasad Vempatapu, Anjan Ray, and Pankaj K
 731 Kanaujia. 2021. 'Application of laccase immobilized rice straw biochar for anthracene
 732 degradation', *Environmental Pollution*, 268: 115827.
- 733 Inbaraj, Baskaran Stephen, Kandi Sridhar, and Bing-Huei Chen. 2021. 'Removal of polycyclic aromatic
 734 hydrocarbons from water by magnetic activated carbon nanocomposite from green tea waste',
 735 *Journal of Hazardous materials*, 415: 125701.
- 736 Isa, Samiratu Atibun, Muhammad Aamir Hafeez, Bhupendra Kumar Singh, Sae Yun Kwon, Sungwook
 737 Choung, and Wooyong Um. 2022. 'Efficient mercury sequestration from wastewaters using palm
 738 kernel and coconut shell derived biochars', *Environmental Advances*, 8: 100196.
- 739 Javanbakht, Vahid, and Zahra Rafiee. 2022. 'Fibrous polyester sponge modified with carboxymethyl
 740 cellulose and Zeolitic imidazolate frameworks for methylene blue dye removal in batch and
 741 continuous adsorption processes', *Journal of Molecular Structure*, 1249: 131552.
- 742 Jiang, Yu, Chen Yang, Qian Yao, Yurong Deng, Jingjing Yang, Yanjun Liu, Zhuozhi Ouyang, Weilin Huang,
 743 and Zhi Dang. 2021. 'Contribution of nitrogen configurations to the adsorption of Cd (ii) in
 744 nitrogen-enriched biochar', *New Journal of Chemistry*, 45: 12669-77.
- 745 Junceda-Mena, Irene, Eduardo García-Junceda, and Julia Revuelta. 2023. 'From the problem to the
 746 solution: Chitosan valorization cycle', *Carbohydrate Polymers*: 120674.
- 747 Kamińska, Gabriela, Mariusz Dudziak, Edyta Kudlek, and Jolanta Bohdziewicz. 2019. 'Preparation,
 748 characterization and adsorption potential of grainy halloysite-CNT composites for anthracene
 749 removal from aqueous solution', *Nanomaterials*, 9: 890.
- 750 Khader, Eman Hashim, Thamer Jassim Mohammed, Nourollah Mirghaffari, Ali Dawood Salman, Tatjana
 751 Juzsakova, and Thamer Adnan Abdullah. 2022. 'Removal of organic pollutants from produced
 752 water by batch adsorption treatment', *Clean Technol Environ Policy*, 24: 713-20.
- 753 Kirmizakis, Panagiotis, Dimitris Kalderis, Dimitrios Ntarlagiannis, and Pantelis Soupios. 2020. 'Preliminary
 754 assessment on the application of biochar and spectral-induced polarization for wastewater
 755 treatment', *Near Surf Geophys*, 18: 109-22.
- 756 Kumar, Jagadeesan Aravind, Duvuru Joshua Amarnath, S Anuradha Jabasingh, Ponnusamy Senthil
 757 Kumar, Kabali Vijai Anand, Gopakumaran Narendrakumar, Selvaraj Karthick Raja Namasivayam,
 758 Thangavelu Krithiga, Samson Sunny, and Somasundaram Purna Pushkala. 2019. 'One pot Green
 759 Synthesis of Nano magnesium oxide-carbon composite: Preparation, characterization and
 760 application towards anthracene adsorption', *J Clean Prod*, 237: 117691.
- 761 Kundu, Sanghamitra, and AK Gupta. 2007. 'Adsorption characteristics of As (III) from aqueous solution
 762 on iron oxide coated cement (IOCC)', *Journal of Hazardous Materials*, 142: 97-104.
- 763 Le Bihanic, Florane, Vivien Sommard, Anaïk Pichon, Julie Grasset, Saadia Berrada, H  l  ne Budzinski,
 764 Xavier Cousin, B  n  dicte Morin, and J  r  me Cachot. 2015. 'Environmental concentrations of
 765 benz [a] anthracene induce developmental defects and DNA damage and impair photomotor
 766 response in Japanese medaka larvae', *Ecotoxicology and Environmental Safety*, 113: 321-28.
- 767 Li, Jun, Zai-lei Yang, Tao Ding, Yi-Jia Song, Hai-Chao Li, De-qiang Li, Sheng Chen, and Feng Xu. 2022. 'The
 768 role of surface functional groups of pectin and pectin-based materials on the adsorption of
 769 heavy metal ions and dyes', *Carbohydrate Polymers*, 276: 118789.
- 770 Li, Xiangcao, Shaojing Zhao, Baoling Li, Ke Yang, Minhuan Lan, and Lintao Zeng. 2021. 'Advances and
 771 perspectives in carbon dot-based fluorescent probes: Mechanism, and application', *Coordination
 772 Chemistry Reviews*, 431: 213686.

- 773 Li, Xiumin, Jingxin Shi, and Xianxin Luo. 2022. 'Enhanced adsorption of rhodamine B from water by Fe-N
774 co-modified biochar: Preparation, performance, mechanism and reusability', *Bioresource*
775 *Technology*, 343: 126103.
- 776 Li, Yage, Sabry M Shaheen, Muhammad Azeem, Lan Zhang, Chuchu Feng, Jin Peng, Weidong Qi, Junxi
777 Liu, Yuan Luo, and Yaru Peng. 2022. 'Removal of lead (Pb²⁺) from contaminated water using a
778 novel MoO₃-biochar composite: Performance and mechanism', *Environmental Pollution*, 308:
779 119693.
- 780 Lin, Xuhui, Wei Wu, and Yirong Mo. 2019. 'How Resonance Modulates Multiple Hydrogen Bonding in
781 Self-Assembled Systems', *J. Org. Chem*, 84: 14805-15.
- 782 Liu, Yiming, Swagata Roy, Samrat Sarkar, Jiaqiang Xu, Yufeng Zhao, and Jiujun Zhang. 2021. 'A review of
783 carbon dots and their composite materials for electrochemical energy technologies', *Carbon*
784 *Energy*, 3: 795-826.
- 785 Lopes, Renata Pereira, and Didier Astruc. 2021. 'Biochar as a support for nanocatalysts and other
786 reagents: Recent advances and applications', *Coordination Chemistry Reviews*, 426: 213585.
- 787 Ma, Ge, Kena Zhang, Haiqing Wang, Zhenda Liang, Li Zhou, and Bing Yan. 2021. 'Versatile synthesis of a
788 highly porous DNA/CNT hydrogel for the adsorption of the carcinogen PAH', *Chemical*
789 *Communications*, 57: 2289-92.
- 790 Madikizela, Lawrence Mzukisi. 2021. 'Removal of organic pollutants in water using water hyacinth
791 (Eichhornia crassipes)', *J. Environ. Manage*, 295: 113153.
- 792 Mansuriya, Bhargav D, and Zeynep Altintas. 2021. 'Carbon Dots: Classification, Properties, Synthesis,
793 Characterization, and Applications in Health Care—An Updated Review (2018–2021)',
794 *Nanomaterials*, 11: 2525.
- 795 Mirzaee, Ehsan, and Majid Sartaj. 2022. 'Activated carbon-based magnetic composite as an adsorbent
796 for removal of polycyclic aromatic hydrocarbons from aqueous phase: Characterization,
797 adsorption kinetics and isotherm studies', *Journal of Hazardous Materials Advances*, 6: 100083.
- 798 Mobarak, Mohamed, Rabea AM Ali, and Moaaz K Seliem. 2021. 'Chitosan/activated coal composite as an
799 effective adsorbent for Mn (VII): Modeling and interpretation of physicochemical parameters',
800 *International Journal of Biological Macromolecules*, 186: 750-58.
- 801 Oh, Seok-Young, and Tae-Cheol Seo. 2019. 'Upgrading biochar via co-pyrolyzation of agricultural
802 biomass and polyethylene terephthalate wastes', *RSC Adv*, 9: 28284-90.
- 803 Ojha, Ankita, and Dhanesh Tiwary. 2021. 'Organic pollutants in water and its health risk assessment
804 through consumption.' in, *Contamination of Water* (Elsevier).
- 805 Okoro, Hussein K, Sadanand Pandey, Clement O Ogunkunle, Catherine J Ngila, C Zvinowanda, Ismaila
806 Jimoh, Isiaka A Lawal, Muiyiwa M Orosun, and Adewale George Adeniyi. 2022. 'Nanomaterial-
807 based biosorbents: Adsorbent for efficient removal of selected organic pollutants from industrial
808 wastewater', *Emerging Contaminants*, 8: 46-58.
- 809 Palansooriya, Kumuduni Niroshika, Sok Kim, Avanthi Deshani Igalavithana, Yohey Hashimoto, Yoon-E
810 Choi, Raj Mukhopadhyay, Binoy Sarkar, and Yong Sik Ok. 2021. 'Fe (III) loaded chitosan-biochar
811 composite fibers for the removal of phosphate from water', *Journal of Hazardous materials*,
812 415: 125464.
- 813 Pathak, Shivangi, Anil Kumar Sakhiya, Abhijeet Anand, KK Pant, and Priyanka Kaushal. 2022. 'A state-of-
814 the-art review of various adsorption media employed for the removal of toxic Polycyclic
815 aromatic hydrocarbons (PAHs): An approach towards a cleaner environment', *J Water Process*
816 *Eng*, 47: 102674.
- 817 Prasannamedha, G, P Senthil Kumar, R Mehala, TJ Sharumitha, and D Surendhar. 2021. 'Enhanced
818 adsorptive removal of sulfamethoxazole from water using biochar derived from hydrothermal
819 carbonization of sugarcane bagasse', *Journal of Hazardous materials*, 407: 124825.

- 820 Qu, Jianhua, Siqi Wang, Yihui Wang, Xue Tian, Zhao Jiang, Yue Tao, Lei Wang, Fengxia Deng, and Ying
821 Zhang. 2021. 'Removal of Cd (II) and anthracene from water by β -cyclodextrin functionalized
822 magnetic hydrochar: Performance, mechanism and recovery', *Bioresource Technology*, 337:
823 125428.
- 824 Ren, Binqiao, Yu Jin, Chongwei Cui, and Xiaoxiao Song. 2022. 'Enhanced Cr (VI) adsorption using
825 chemically modified dormant *Aspergillus niger* spores: process and mechanisms', *Journal of
826 environmental chemical engineering*, 10: 106955.
- 827 Ren, Xinhao, Fei Wang, Fengmei Cao, Junkang Guo, and Hongwen Sun. 2018. 'Desorption of atrazine in
828 biochar-amended soils: effects of root exudates and the aging interactions between biochar and
829 soil', *Chemosphere*, 212: 687-93.
- 830 Saad, Mouhamed El Khames, Ramzi Khiari, Elimame Elaloui, and Younes Moussaoui. 2014. 'Adsorption
831 of anthracene using activated carbon and *Posidonia oceanica*', *Arab J Chem* 7: 109-13.
- 832 Saad, Naim, Maya Chaaban, Digambara Patra, Aline Ghanem, and Houssam El-Rassy. 2020. 'Molecularly
833 imprinted phenyl-functionalized silica aerogels: Selective adsorbents for methylxanthines and
834 PAHs', *Microporous and Mesoporous Materials*, 292: 109759.
- 835 Saheed, Ismaila Olalekan, Wen Da Oh, and Faiz Bukhari Mohd Suah. 2021. 'Chitosan modifications for
836 adsorption of pollutants—A review', *Journal of Hazardous materials*, 408: 124889.
- 837 Shaheen, Sabry M, Ahmed Mosa, Hamada Abdelrahman, Nabeel Khan Niazi, Vasileios Antoniadis,
838 Muhammad Shahid, Hocheol Song, Eilhann E Kwon, and Jörg Rinklebe. 2022. 'Removal of toxic
839 elements from aqueous environments using nano zero-valent iron-and iron oxide-modified
840 biochar: a review', *Biochar*, 4: 1-21.
- 841 Shaikh, Wasim Akram, Md Arsh Alam, Md Osaid Alam, Sukalyan Chakraborty, Gary Owens, Tanushree
842 Bhattacharya, and Naba Kumar Mondal. 2020. 'Enhanced aqueous phase arsenic removal by a
843 biochar based iron nanocomposite', *Environmental Technology & Innovation*, 19: 100936.
- 844 Shaikh, Wasim Akram, Sukalyan Chakraborty, Rafique Ul Islam, Ayman A Ghfar, M Naushad, Jochen
845 Bundschuh, Jyoti Prakash Maity, and Naba Kumar Mondal. 2022. 'Fabrication of biochar-based
846 hybrid Ag nanocomposite from algal biomass waste for toxic dye-laden wastewater treatment',
847 *Chemosphere*, 289: 133243.
- 848 Shaikh, Wasim Akram, Rafique Ul Islam, and Sukalyan Chakraborty. 2021. 'Stable silver nanoparticle
849 doped mesoporous biochar-based nanocomposite for efficient removal of toxic dyes', *Journal of
850 environmental chemical engineering*, 9: 104982.
- 851 Shaikh, Wasim Akram, Abhishek Kumar, Sukalyan Chakraborty, Rafique Ul Islam, Tanushree
852 Bhattacharya, and Jayanta Kumar Biswas. 2022. 'Biochar-based nanocomposite from waste tea
853 leaf for toxic dye removal: From facile fabrication to functional fitness', *Chemosphere*, 291:
854 132788.
- 855 Shaikh, Wasim Akram, Abhishek Kumar, Sukalyan Chakraborty, Mu Naushad, Rafique Ul Islam,
856 Tanushree Bhattacharya, and Saugata Datta. 2022. 'Removal of toxic dye from dye-laden
857 wastewater using a new nanocomposite material: Isotherm, kinetics and adsorption
858 mechanism', *Chemosphere*, 308: 136413.
- 859 Singh, Santosh, Himanshu Gupta, Soniya Dhiman, and Nawal Kishore Sahu. 2022. 'Decontamination of
860 cationic dye brilliant green from the aqueous media', *Applied Water Science*, 12: 1-10.
- 861 Singh, SK, and RK Singh. 2023. 'An overview on remediation technologies for polycyclic aromatic
862 hydrocarbons in contaminated lands: a critical approach', *Environment, Development and
863 Sustainability*: 1-35.
- 864 Song, Tiantian, Weijun Tian, Jing Zhao, Kaili Qiao, Mengyuan Zou, and Meile Chu. 2021. 'N-doped
865 Reduced Graphene Oxide nanocomposites encapsulated sodium alginate/polyvinyl alcohol
866 microspheres for anthracene and its oxygenated-PAH removal in aqueous solution', *J Taiwan
867 Inst Chem Eng*, 125: 168-75.

- 868 Sun, Ying, Lili Zheng, Xiaoyan Zheng, Dao Xiao, Yang Yang, Zhengke Zhang, Binling Ai, and Zhanwu Sheng.
869 2022. 'Adsorption of sulfonamides in aqueous solution on reusable coconut-shell biochar
870 modified by alkaline activation and magnetization', *Frontiers in Chemistry*, 9: 1274.
- 871 Tang, Rongdi, Daoxin Gong, Yaocheng Deng, Sheng Xiong, Jiangfu Zheng, Ling Li, Zhanpeng Zhou, Long
872 Su, and Jia Zhao. 2022. ' π - π stacking derived from graphene-like biochar/g-C₃N₄ with tunable
873 band structure for photocatalytic antibiotics degradation via peroxymonosulfate activation',
874 *Journal of Hazardous materials*, 423: 126944.
- 875 Tirado-Guizar, Antonio, William González-Gómez, Georgina Pina-Luis, José Trinidad Elizalde Galindo, and
876 Francisco Paraguay-Delgado. 2020. 'Anthracene removal from water samples using a composite
877 based on metal-organic-frameworks (MIL-101) and magnetic nanoparticles (Fe₃O₄)',
878 *Nanotechnology*, 31: 195707.
- 879 Usman, Muhammad, Adeel Ahmed, Bing Yu, Song Wang, Youqing Shen, and Hailin Cong. 2021.
880 'Simultaneous adsorption of heavy metals and organic dyes by β -Cyclodextrin-Chitosan based
881 cross-linked adsorbent', *Carbohydrate Polymers*, 255: 117486.
- 882 Valderrama, C, X Gamisans, X De las Heras, A Farran, and JL Cortina. 2008. 'Sorptions kinetics of polycyclic
883 aromatic hydrocarbons removal using granular activated carbon: intraparticle diffusion
884 coefficients', *Journal of Hazardous materials*, 157: 386-96.
- 885 Valizadeh, Soheil, Sang Soo Lee, Yong Jun Choi, Kitae Baek, Byong-Hun Jeon, Kun-Yi Andrew Lin, and
886 Young-Kwon Park. 2022. 'Biochar application strategies for polycyclic aromatic hydrocarbons
887 removal from soils', *Environmental research*, 213: 113599.
- 888 Verma, Monu, Ingyu Lee, Youngmin Hong, Vinod Kumar, and Hyunook Kim. 2022. 'Multifunctional β -
889 cyclodextrin-EDTA-chitosan polymer adsorbent synthesis for simultaneous removal of heavy
890 metals and organic dyes from wastewater', *Environmental Pollution*, 292: 118447.
- 891 Wade, Jr Leroy G, and Jan William Simek. 2017. *Organic Chemistry, 9e* (Pearson Education India).
- 892 Wang, Jianlong, and Shizong Wang. 2019. 'Preparation, modification and environmental application of
893 biochar: A review', *Journal of Cleaner Production*, 227: 1002-22.
- 894 Wang, Tong, Jie He, Jian Lu, Yi Zhou, Zhaohui Wang, and Yanbo Zhou. 2021. 'Adsorptive removal of
895 PPCPs from aqueous solution using carbon-based composites: A review', *Chinese Chemical
896 Letters*.
- 897 Wiśniowska, Ewa, and Maria Włodarczyk-Makuła. 2022. 'Evaluation of the adsorption efficiency of
898 carcinogenic PAHs on microplastic (polyester) fibers—preliminary results', *Appl Water Sci*, 12: 1-
899 7.
- 900 Wu, Weilong, Zihan Liu, Muhammad Azeem, Zhiqiang Guo, Ronghua Li, Yage Li, Yaru Peng, Esmat F Ali,
901 Hailong Wang, and Shengsen Wang. 2022. 'Hydroxyapatite tailored hierarchical porous biochar
902 composite immobilized Cd (II) and Pb (II) and mitigated their hazardous effects in contaminated
903 water and soil', *Journal of Hazardous materials*: 129330.
- 904 Xue, Shuwen, Yawen Xiao, Guoqiang Wang, Jinjin Fan, Keji Wan, Qiongqiong He, Mingqiang Gao, and
905 Zhenyong Miao. 2021. 'Adsorption of heavy metals in water by modifying Fe₃O₄ nanoparticles
906 with oxidized humic acid', *Colloids Surf A Physicochem Eng Asp*, 616: 126333.
- 907 Yuan, Jieming, Yinghao Wen, Dionysios D Dionysiou, Virender K Sharma, and Xingmao Ma. 2022.
908 'Biochar as a novel carbon-negative electron source and mediator: electron exchange capacity
909 (EEC) and environmentally persistent free radicals (EPFRs): a review', *Chemical Engineering
910 Journal*, 429: 132313.
- 911 Zango, Zakariyya Uba, Khairulazhar Jumbri, Nonni Soraya Sambudi, Noor Hana Hanif Abu Bakar, Nor Ain
912 Fathihah Abdullah, Chanbasha Basheer, and Bahruddin Saad. 2019. 'Removal of anthracene in
913 water by MIL-88 (Fe), NH₂-MIL-88 (Fe), and mixed-MIL-88 (Fe) metal-organic frameworks', *RSC
914 Adv*, 9: 41490-501.

- 915 Zhang, Kun, Baoliang Chen, Jiefei Mao, Lizhong Zhu, and Baoshan Xing. 2018. 'Water clusters
916 contributed to molecular interactions of ionizable organic pollutants with aromatized biochar via
917 π -PAHB: sorption experiments and DFT calculations', *Environmental Pollution*, 240: 342-52.
- 918 Zhang, Wei, Ji Ou, Bin Wang, Hongyu Wang, Qiulai He, Jianyang Song, Huining Zhang, Meiyi Tang, Lean
919 Zhou, and Yang Gao. 2021. 'Efficient heavy metal removal from water by alginate-based porous
920 nanocomposite hydrogels: The enhanced removal mechanism and influencing factor insight',
921 *Journal of Hazardous materials*, 418: 126358.
- 922 Zhang, Yanfeng, Jun Yin, Zhiqian Qv, Huijuan Chen, Hongwei Li, Ying Zhang, and Lingyan Zhu. 2022.
923 'Deriving freshwater sediment quality guidelines of polycyclic aromatic hydrocarbons using
924 method of species sensitivity distribution and application for risk assessment', *Water Research*,
925 225: 119139.
- 926 Zhang, Yue, Xiaoyun Xu, Lingzhi Cao, Yong Sik Ok, and Xinde Cao. 2018. 'Characterization and
927 quantification of electron donating capacity and its structure dependence in biochar derived
928 from three waste biomasses', *Chemosphere*, 211: 1073-81.
- 929 Zhao, Nan, Chuanfang Zhao, Kunyuan Liu, Weihua Zhang, Daniel CW Tsang, Zaikuan Yang, Xixiang Yang,
930 Bofang Yan, Jean Louis Morel, and Rongliang Qiu. 2021. 'Experimental and DFT investigation on
931 N-functionalized biochars for enhanced removal of Cr (VI)', *Environmental Pollution*, 291:
932 118244.
- 933 Zhou, Xinxing, Liang Shi, Taher Baghaee Moghaddam, Meizhu Chen, Shaopeng Wu, and Xiangzhou Yuan.
934 2022. 'Adsorption mechanism of polycyclic aromatic hydrocarbons using wood waste-derived
935 biochar', *Journal of Hazardous materials*, 425: 128003.
- 936 Zhu, Lingli, Dekui Shen, Qian Liu, Chunfei Wu, and Sai Gu. 2021. 'Sustainable synthesis of bright green
937 fluorescent carbon quantum dots from lignin for highly sensitive detection of Fe³⁺ ions', *Applied*
938 *Surface Science*, 565: 150526.
- 939